IVYSPRING INTERNATIONAL PUBLISHER

Theranostics

2023; 13(7): 2114-2139. doi: 10.7150/thno.80213

Review

Bench–to–bedside development of multifunctional flexible embolic agents

Dawei Wang[1,2,3]✉, and Wei Rao[1,2,3,]✉

1. Key Lab of Cryogenics, Technical Institute of Physics and Chemistry, Chinese Academy of Sciences, Beijing, 100190, China
2. Beijing Key Lab of CryoBiomedical Engineering, Technical Institute of Physics and Chemistry, Chinese Academy of Sciences, Beijing, 100190, China
3. School of Future Technology, University of Chinese Academy of Sciences, Beijing 100049, China

✉ Corresponding author: Dr. Dawei Wang. wangdawei181@mails.ucas.ac.cn; Pro. Wei Rao. weirao@mail.ipc.ac.cn.

© The author(s). This is an open access article distributed under the terms of the Creative Commons Attribution License (https://creativecommons.org/licenses/by/4.0/). See http://ivyspring.com/terms for full terms and conditions.

Received: 2022.10.26; Accepted: 2022.12.22; Published: 2023.04.01

Abstract

Transarterial chemoembolization (TACE) has been demonstrated to provide a survival benefit for patients with unresectable hepatocellular carcinoma (HCC). However, conventional TACE still faces limitations associated with complications, side effects, unsatisfactory tumor responses, repeated treatment, and narrow indications. For further improvement of TACE, additional beneficial functions such as degradability, drug–loading and releasing properties, detectability, targetability, and multiple therapeutic modalities were introduced. The purpose here is to provide a comprehensive overview of current and emerging particulate embolization technology with respect to materials. Therefore, this review systematically identified and described typical features, various functions, and practical applications of recently emerging micro/nano materials as particulate embolic agents for TACE. Besides, new insights into the liquid metals–based multifunctional and flexible embolic agents were highlighted. The current development routes and future outlooks of these micro/nano embolic materials were also presented to promote advancement in the field.

Keywords: Hepatocellular carcinoma (HCC); Transarterial chemoembolization (TACE); Micro/nano materials; Particulate embolic agents; Ga based liquid metal; Multifunctional flexible embolic agents

1. Introduction

Hepatocellular carcinoma (HCC) is one of the most frequently diagnosed primary liver cancer and is becoming one of the leading causes of cancer–related mortality because of complex tumor pathogenesis, disease recurrence, and metastases [1-3]. Despite significant advances in screening, diagnosis, and treatment, patients with HCC still face a poor prognosis with a 5–year survival rate of approximately 10% to 15% [2, 4]. This could be interpreted by the fact that although the surveillance programs of at–risk populations are widely implemented, most patients with HCC are first diagnosed at an intermediate or advanced stage (Barcelona Clinic Liver Cancer stage B or C) [2, 5] when curative treatments such as surgical excision, liver transplantation and percutaneous ablation (radiofrequency ablation, microwave ablation, etc.) cannot be applied [6-14]. Therefore, the preferred treatment for patients with advanced–stage HCC is topical or palliative treatment rather than curative treatment. Recently, the importance of interventional treatment is increasing for patients with advanced–stage HCC [15], because of superior features such as substantially reduced therapeutic complication, minimally invasive, delaying disease progression and corresponding improved life quality. Among them, transarterial chemoembolization (TACE) is one of the most critical palliative treatment options for inoperable HCC [8, 16-19], which can also be implemented as a preoperative adjuvant treatment for patients with resectable HCC [15, 20].

Viral infections, genetic disorders, chemical toxins, and metabolic syndrome are the main factors contributing to the development of HCC, which can modulate oxidative stress, cancer stem cells, hypoxia,

hormonal system, inflammatory/immune system and epithelial-mesenchymal transition [21-23]. After tumorigenesis, the growth and metastasis of invasive tumors depend on tumor angiogenesis [24, 25], and their evolution can be divided into three stages (as illustrated in Figure 1). First, a tumor appears in the liver and starts to grow by obtaining nutrients from its immediate environment. When growing to a certain size, the tumor will secrete proangiogenic factors to accelerate neovascularization (referred to as angiogenesis) due to ischemia and a decrease of pH in local tissues, thus providing oxygen and nutrients required for tumor growth. Finally, the tumor becomes invasive while the tumor cells may spread to other organs. Because of the unique evolutionary process of HCC, TACE can inhibit tumor growth and metastasis by cutting off the pathways of oxygen, nutrient, and tumor cell transmission.

The schematic diagram of the TACE procedure was shown in Figure 2. Briefly, the embolic materials and chemotherapeutic agents are selectively injected into the targeted tumor vessels under the guidance of precise imaging assistance, then the supply of nutrients and oxygen is cut off and the chemotherapeutic drugs are released, ultimately causing ischemia, necrosis, and chemo–toxicity to the tumor cells [26-29]. TACE can treat HCC without affecting normal hepatic parenchyma, because of the difference in blood supply between hypervascular tumors (mainly from the hepatic artery [30, 31]) and normal liver tissue (unique dual blood supply, namely: two–thirds of the necessary blood supply comes from the portal vein and one–third from hepatic artery [26]). However, not every patient with HCC may benefit from TACE. Considering tumor size, tumor location, extrahepatic spread, underlying liver function, and patient status, etc [12], the best candidates who may benefit from TACE are patients with asymptomatic lesions and preserved liver function without extrahepatic spread or vascular invasion [32]. The optimum treatments need to be carefully selected for the individual patient, such as blank transarterial embolization (TAE), conventional transarterial chemoembolization (cTACE), TACE with drug–eluting beads (DEB–TACE), transarterial radioembolization (TARE), arterial embolization hyperthermia (AEH) and other treatments in combination with TACE. Transcatheter vascular occlusion can be achieved by using multiplex forms of embolic agents, including devices (e.g., coils, stents, and balloons), liquids (e.g., glue and *in situ* gelling solution), sclerosing agents (e.g., alcohol and thrombin) and particulates (e.g., polymer and hydrogels particulates) [33, 34]. Among them, particulates are becoming ideal embolic agents for integrated and tailored transarterial embolization therapy, due to their versatile functionality [35].

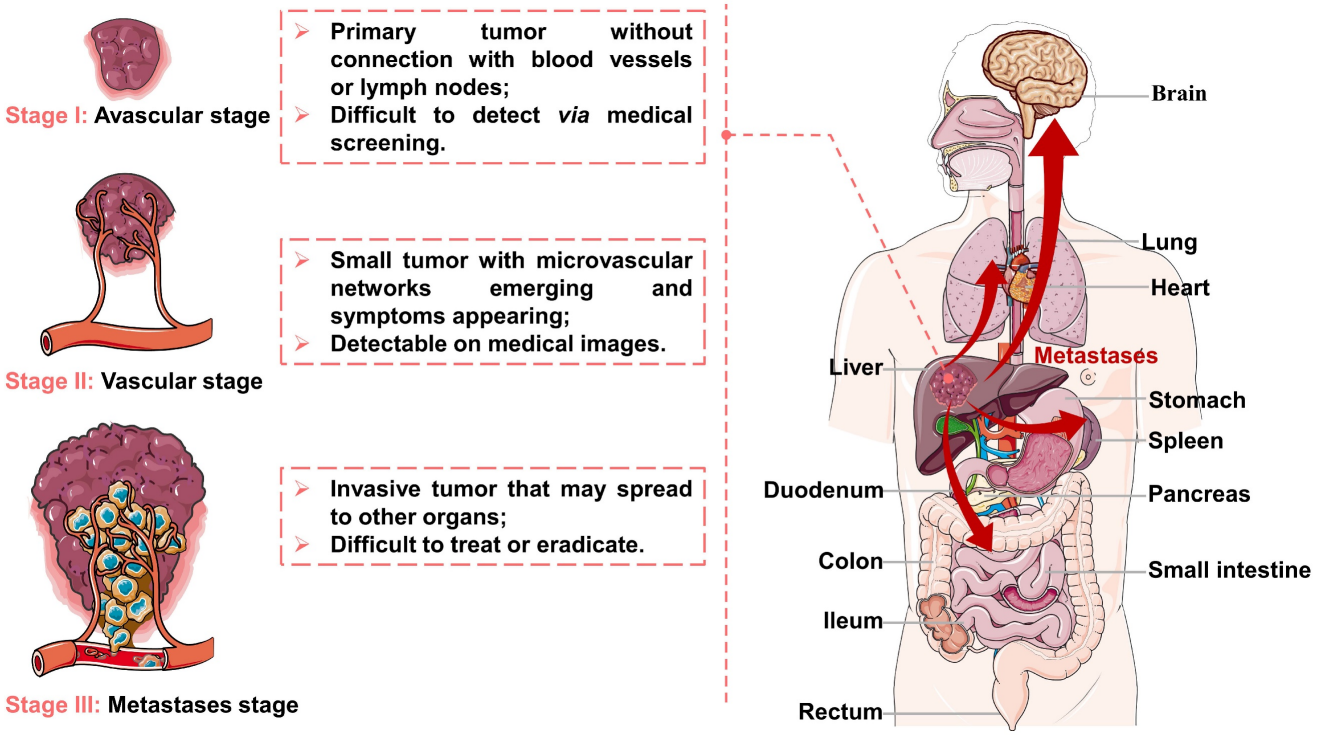

Figure 1. Representation of the liver cancer stages: (I) avascular stage; (II) vascular stage; (III) metastases stage. Created in Smart.Servier.com.

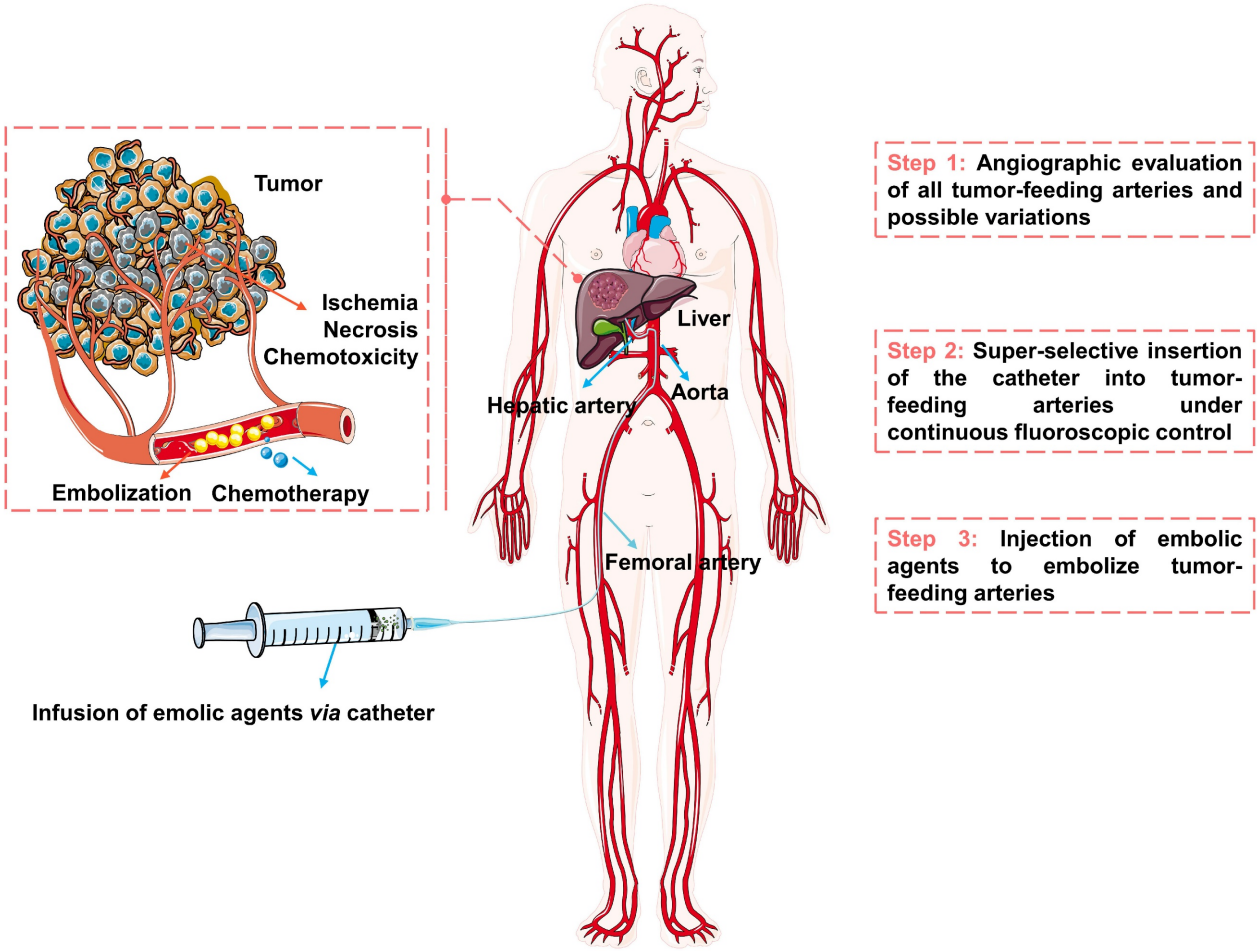

Figure 2. The schematic diagram of transarterial embolization for hepatocellular carcinoma. Created in Smart.Servier.com.

Nowadays, with the innovation of micro/nano technology and material design, more and more micro/nano embolic particulates (materials: polymeric, metallic, natural, or composite; structure: non-spherical, spherical, porous, capsule, hollow or shell-core type) are emerging (Figure 3A). Since the innovation of materials will eventually exert the diagnostic and therapeutic functions of embolic agents. Therefore, this review systematically identified and described recently emerging micro/nano materials as particulate embolic agents for TACE, with emphasis on materials, typical features, various functions, and practical applications (Figure 3B). The content began with a description of the basic embolic matrix, followed by a detailed introduction of the typical embolic microspheres used clinically (e.g., drug-eluting beads, imageable embolic microspheres, and radioactive microspheres). Then, the vision was expanded to the stimuli-sensitive embolic microspheres in terms of properties, performances, and underlying application (e.g., combination therapy of TACE with various interventional thermal/nonthermal ablation modalities). After that, new insights into the liquid metals-based multifunctional flexible embolic agents were presented, which are expected to have a broader impact on future angiography and intravascular embolization. Finally, the current development routes and future outlooks of these emerging micro/nano embolic materials were also concluded.

2. Micro/nano materials used for particulate embolic agents

2.1 Simple embolic agents for TAE or cTACE

Conventional transarterial chemoembolization TACE (cTACE) typically involves the sequential infusion of chemotherapeutic agents mixed with Lipiodol and embolic agents into the tumor-feeding hepatic artery branch, while blank transarterial embolization (TAE) aims to achieve devascularization in absence of chemotherapeutic agents [15, 19, 36-39]. The embolic agents implanted in the tumor-feeding vessels provide a single but fundamental function of embolization. Simple embolic agents include: (1) biodegradable embolic agents for temporary embolization, e.g., albumin, gelatin, starch, dextran, chitosan, alginate, carboxymethyl cellulose, polylactic-co-

glycolic acid (PLGA), polyanhydride, and polyesters, etc. [40], and (2) nonbiodegradable embolic agents for permanent embolization, e.g., polyvinyl alcohol (PVA) particles, trisacryl gelatin particles, and derivative particles. The common feature of these basic embolic agents is their good biocompatibility, and they are often used as matrix materials to prepare various functional embolic agents, especially those currently under investigation.

2.1.1 Temporary gelatin–based embolic agents

Autologous blood clots were the first developed temporary embolic materials for endovascular embolization, after that, autologous subcutaneous muscle and tissue were also used as embolic materials [41, 42]. These naturally autologous embolic materials are nontoxic and biocompatible because they can be individualized for each patient [42]. However, they are rarely used in current clinical due to the increasing clinical demand and the rapid advancements in particle embolization technology. The currently available gelatin–based embolic agents (various forms: gelatin foam, gelatin powder, gelatin microspheres, etc.) are derived from purified porcine gelatin (non–antigenic carbohydrate), which can be enzymatically digested for temporary embolization. The gelatin–based embolic agents mechanically embolize tumor arteries to block or retard blood flow, while the internal reticular structure can enhance the embolization effect by promoting thrombus formation (reticulating the red blood cells and platelets). Gelatin foams are one of the common embolic agents [16, 43], which have been introduced for TAE in the late 1970s [44, 45]. Gelatin foams are often marketed as Gelfoam (e.g., Pharmacia & Upjohn Co., New York), and are available in different configurations (e.g., sponges and sterile sheets) with typical particle sizes range of 0.5~2 mm [46]. During embolization, the injectable slurry is formed through the physical mixing of the gelatin foams with the iodinated contrast media (for radiopacity) [36, 47]. Additionally, gelatin foams as hemostatic embolic agents can promote blood clotting and reduce blood loss, and its porous structure can be a scaffold to promote cell adhesion and tissue regeneration [34]. Millimeter–scaled gelatin foams are likely to clump in larger arteries, and thus cannot penetrate the smaller vessels in distal tissues. Although micron–sized gelatin powder (size ranging from 40 to 60 μm [34]) can reach smaller vessels to achieve more distal vessel obstruction, it is more likely to cause insufficient or non-targeted embolization [48-50]. Furthermore, gelatin microspheres with regular shapes and variable diameters (ranging from 40 to 1200 μm) have also been produced, such as: gelatin sponge microparticles (GSMs) [51], and gelatin microparticles (GMPs) [29]. The gelatin microspheres with accurate particle size can effectively avoid ectopic embolization, which is crucial for localized, targeted, and tailored embolization. Due to the degradable nature of the gelatin matrix, the vessel recanalization may occur within a few weeks, showing advantages in hepatic TAE/cTACE and facilitating repeated intra–arterial treatment [29]. However, uncontrolled degradation kinetics of these gelatin embolic particles may cause uncertainties in clinical trials, thus hindering their widespread application.

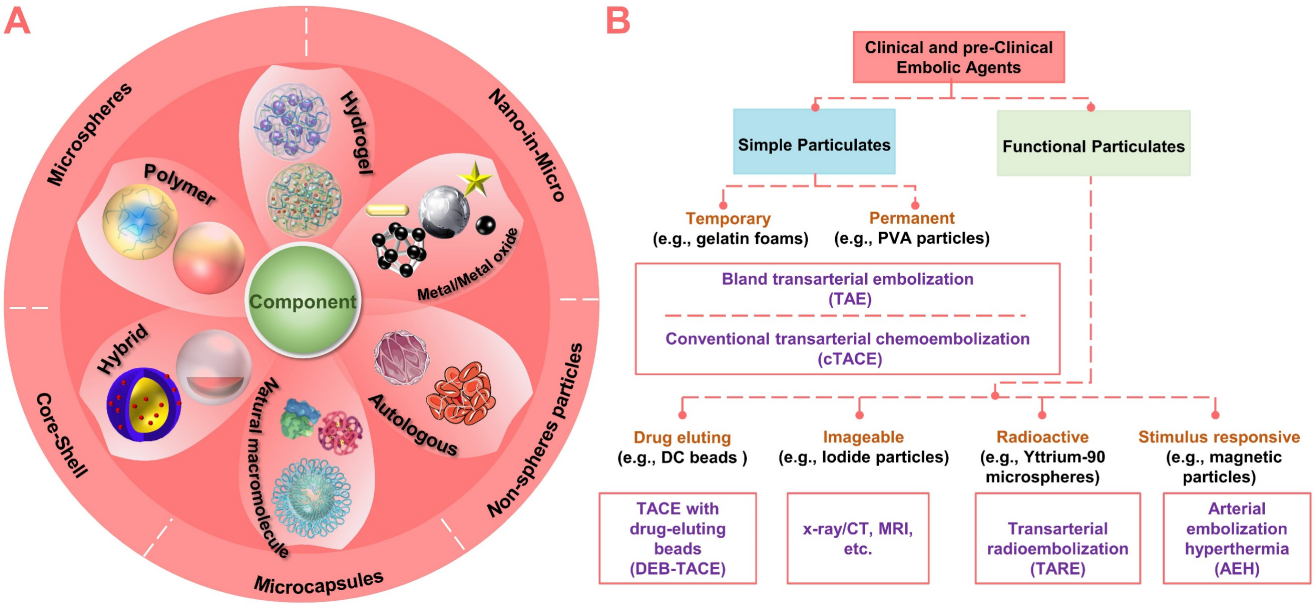

Figure 3. Summary of clinical and pre–clinical particulate embolic agents. (A) Structure and component of micro/nano embolic agents. (B) Classification of micro/nano embolic agents.

2.1.2 Permanent PVA–based embolic agents

Polyvinyl alcohol (PVA)–based particles are mature polymeric embolic agents with good safety, long–term biocompatibility, and non–biodegradability, which can be used for permanent or semi–permanent embolization. The initially used PVA particles were obtained by mechanically fragmenting, screening, and separating the PVA polymer blocks [52], which were used as vascular embolic agents in clinical practice since the 1970s [53]. When injected into tumor–feeding arteries, the PVA particles can also achieve devascularization followed by thrombus formation. Different from temporary embolic agents, the recanalization in PVA particles–mediated TAE/cTACE may occur over several months due to particle migration and vascular remodeling [54]. However, due to irregular shapes, inhomogeneous sizes [55], and charged/hydrophobic surfaces [34], the PVA particles are prone to aggregate and thus may lead to catheter occlusion [56] or accidental blockage of the proximal larger vessels [57]. The main challenge is the unpredictable embolic behavior caused by the dimension uncertainty between the PVA particles and the target tumor–feeding arteries [34]. For this reason, several vendors have developed PVA–based microspheres with regular shapes and dimensional accuracy. For example, spherical PVA microspheres (Contours SE, Boston Scientific, Natick, MA), PVA microspheres crosslinked with acrylic polymer (Bead Block, Biocompatibles UK, Surrey), and PVA microspheres with hydrogel core (LC Bead, Biocompatibles Inc. and RITA, Manchester, GA), which are commercially available with sizes ranges of 100–300, 300–500, 500–700, and 700–900 μm [58]. With structural optimization and surface modification, these PVA–based microspheres may overcome some of the disadvantages related to PVA particles, providing more precise treatment control.

2.2 Drug–eluting beads for DEB–TACE

During the cTACE, although the dual efficacy of chemotherapy and embolization can be achieved, there are still shortcomings associated with complications, side effects, and unsatisfactory treatment responses, such as insufficient or nontarget embolization [59], uncontrolled and unsustainable chemotherapeutic drug release [19, 60], ineffective drugs concentration in tumor tissue [60], and high incidence of liver–related systemic toxicities [17, 38, 61], etc. The newer drug–eluting beads (DEBs)–mediated TACE (DEB–TACE) utilizes a single delivery system of DEBs [62], which can reduce the concentration of chemotherapeutic drugs in systemic circulation and maintain effective drug concentration within the target tumor for a prolonged period [60, 63], showing less systemic side effects [64] and more benefits over cTACE according to clinical studies [36, 39]. In particular, the TACE procedure could also be significantly simplified since the DEBs play a dual role, acting as both an embolic agent and a drug carrier [65]. So far, a variety of DEBs or also called drug–eluting microspheres (DEMs) have been developed, and some are commercially available (Table 1). And there are also many anti–tumor drugs available for TACE (such as doxorubicin, epirubicin, idarubicin, mitoxantrone, carboplatin, cisplatin, oxaliplatin, 5–fluorouracil, gemcitabine, mitomycin C, and paclitaxel, etc. [66]), among which doxorubicin is one of the most commonly used in clinic [67]. It should be noted that under TACE–induced ischemic stress, retention of hypoxia-inducible factor 1 (HIF–1), upregulation of angiogenic receptors, and increased nuclear proliferation rates may occur within embolized tumor tissue [68]. Among them, HIF–1 as a controlling factor may regulate the subsequent release of multiple angiogenic factors (such as vascular endothelial growth factor, insulin–like growth factor and basic fibroblast growth factor), thereby inducing angiogenesis [21, 69]. Fortunately, anti–angiogenic drugs (e.g., sorafenib) could also be combined with DEB–TACE to inhibit the induction of HIF–1, while favorable tumor inhibition rate has been demonstrated in phase–II trials for patients with unresectable HCC [70]. The matrix of DEBs is a critical determinant of the drug loading and releasing mechanisms [71], while the microstructure (e.g., porosity) is another factor that modulates drug loading and releasing profiles [72]. Thus, we will discuss the typical DEBs mainly based on the drug loading and releasing mechanisms.

2.2.1 Drug–eluting beads based on ion–exchange mechanism

This type of negatively charged DEBs are capable of loading and eluting positively charged chemotherapeutic agents *via* an ion–exchange mechanism (Figure 4A) [18]. Among them, the commercially available DC Beads are the most commonly used and well–characterized in DEB–TACE for HCC [75, 76]. DC beads are typically available with size ranges of 100–300, 300–500, 500–700, and 700–900 μm (Table 1), and are generally supplied in the hydrated form (in saline solution with appropriate ionic strength). In particular, DC Beads are PVA–based microspheres containing anionic sulfonate groups that allow the sequestering of positively charged drugs, such as doxorubicin, and irinotecan, *via* Coulomb charge interactions [26].

Table 1. Summary of commercially available drug–eluting beads [18, 56, 73, 74].

Product name	DC Bead®	HepaSphere®	Tandem®	LifePearl®
Company	BTG, London, UK	Merit Medical, South Jordan, UT, USA	CeloNova BioSciences, Inc., San Antonio, TX, USA	Terumo European Interventional Systems, Leuven, Belgium
Materials composition	Acrylamido–polyvinylalcohol–AMPS hydrogel microspheres	Poly (vinyl alcohol–co–acrylic acid) microspheres	Poly (methylacrylic acid) microspheres coated with Polyzene–F	Polyethylene glycol–AMPS based microspheres
Available size (μm)	70–150, 100–300, 300–500, 500–700	30–60, 50–100, 100–150, 150–200	40, 75, 100, 250, 400, 500, 700, 900	100, 200, 400
Specific properties	Spherical, calibrated sizes, nonabsorbable, contain sulfonate binding groups	Calibrated, dry microspheres, absorbable, contain carboxylate binding groups	Spherical, calibrated sizes, nonabsorbable, contain carboxylate binding groups	Spherical, calibrated sizes, nonabsorbable, tinted green, contain sulfonate binding groups
Drug type	Doxorubicin and irinotecan	Doxorubicin, irinotecan, epirubicin, cisplatin or oxaliplatin	Doxorubicin and irinotecan	Doxorubicin, irinotecan, idarubicin, and epirubicin
Drug loading efficiency (maximum doses)	Doxorubicin (37.5 mg mL^{-1}) and irinotecan (50 mg mL^{-1})	Doxorubicin (3 mg mg^{-1} of microspheres) and irinotecan (4 mg mg^{-1} of microspheres)	Doxorubicin (50 mg mL^{-1}) and irinotecan (50 mg mL^{-1})	Doxorubicin (37.5 mg mL^{-1}), irinotecan (50 mg mL^{-1}), idarubicin (5 mg mL^{-1}) and epirubicin (25 mg mL^{-1})

In order to load the drugs into the DC beads, it is necessary to remove the saline solution before TACE treatment, and then mixed with the drug solution for an appropriate time (as the loading process outlined in Figure 4A) [65]. When loading with doxorubicin (red), the DC beads will gradually turn red with associated shrinkage, while the red coloration in the solution will diminish (Figure 4A). Up to 99% of doxorubicin uptake occurs between 20 min and 24 h, depending on loading concentration and bead size. In addition, DC beads also show advantages in drug elution performance compared to traditional Lipiodol–doxorubicin emulsions (Figure 4C), sustained–release Vs. rapid–release). The underlying mechanisms may be that the elution kinetics of DC beads are primarily governed by the ionic environment and surface area, since ions need to penetrate the surface and diffuse into the hydrogel matrix to displace the drugs from the sulfonate moieties (Figure 4C, i) [65, 77, 78]. In comparison, the water–soluble drugs will be rapidly released from the Lipiodol–doxorubicin emulsions, as the Lipiodol droplets will rapidly separate from the emulsion (Figure 4C, ii) [65, 77]. Furthermore, the clinical researches have shown that the high drug–loading efficacy and targeted/sustained drug–releasing properties of DC beads did contribute to improved response (higher rates of complete response, objective response, and disease control) and tolerability (significant reduction in severe liver toxicity and significantly lower rate of doxorubicin–related side effects) compared to cTACE in HCC patients [76, 79]. However, the DC beads with the negatively charged surface can only load cationic drugs and the non–biodegradable nature may also lead to late–stage inflammatory responses due to persistent occlusion [80].

2.2.2 Drug–eluting beads based on swelling mechanism

In order to expand the types of drugs that can be loaded by DEBs, the absorption properties of the gel materials have been developed, so that anionic drugs can be loaded *via* a swelling mechanism (Figure 4B). As a typical example, HepaSphere microspheres are hydrophilic, superabsorbent polymer microspheres, which can be bound with doxorubicin, irinotecan, epirubicin, cisplatin or oxaliplatin [81]. HepaSphere microspheres are available in the 'dry state' with size ranges of 50–100, 100–150, and 150–200 μm (Table 1). When exposed to aqueous–based media, the dry HepaSphere microspheres may undergo dramatic morphological changes after absorbing liquid (e.g., becoming soft, deformable, and accompanied by volume expansion (up to 64 × volume [32])). Due to the high degree of compliance and flexibility, the hydrated HepaSphere microspheres can be easily delivered through the currently available microcatheters [26], and can match the shape of tortuous and narrow vessels for a more complete embolization [81, 82]. In contrast with DC Beads, the HepaSphere microspheres also possess a negative ionic charge, which allows the binding of cationic drug molecules *via* electrostatic interactions (Figure 4B) [81-83]. However, due to the porous structure of the HepaSphere microspheres, the chemotherapeutic drugs are bound throughout the volume, while the DC Beads are on the surface (Figure 4A–B) [81, 83]. A comparative study by Jordan O et al. has shown that the doxorubicin loading efficiency and releasing profile of HepaSphere microspheres (400–600 μm) was similar to that of DC Beads (500–700 μm) [83]. They observed incomplete release of doxorubicin in saline (release rate over 1 week: 27 ± 2 % for DC beads and 18 ± 7 % for HepaSphere microspheres; P = 0.013), which may explain the low systemic exposure and suboptimal anticancer function of doxorubicin [81, 83]. Besides, they also observed some fractured HepaSphere microspheres after drug release [83]. In short, the HepaSphere microspheres are also an appropriate option in DEB–TACE for HCC, showing favorable safety and efficacy [84, 85].

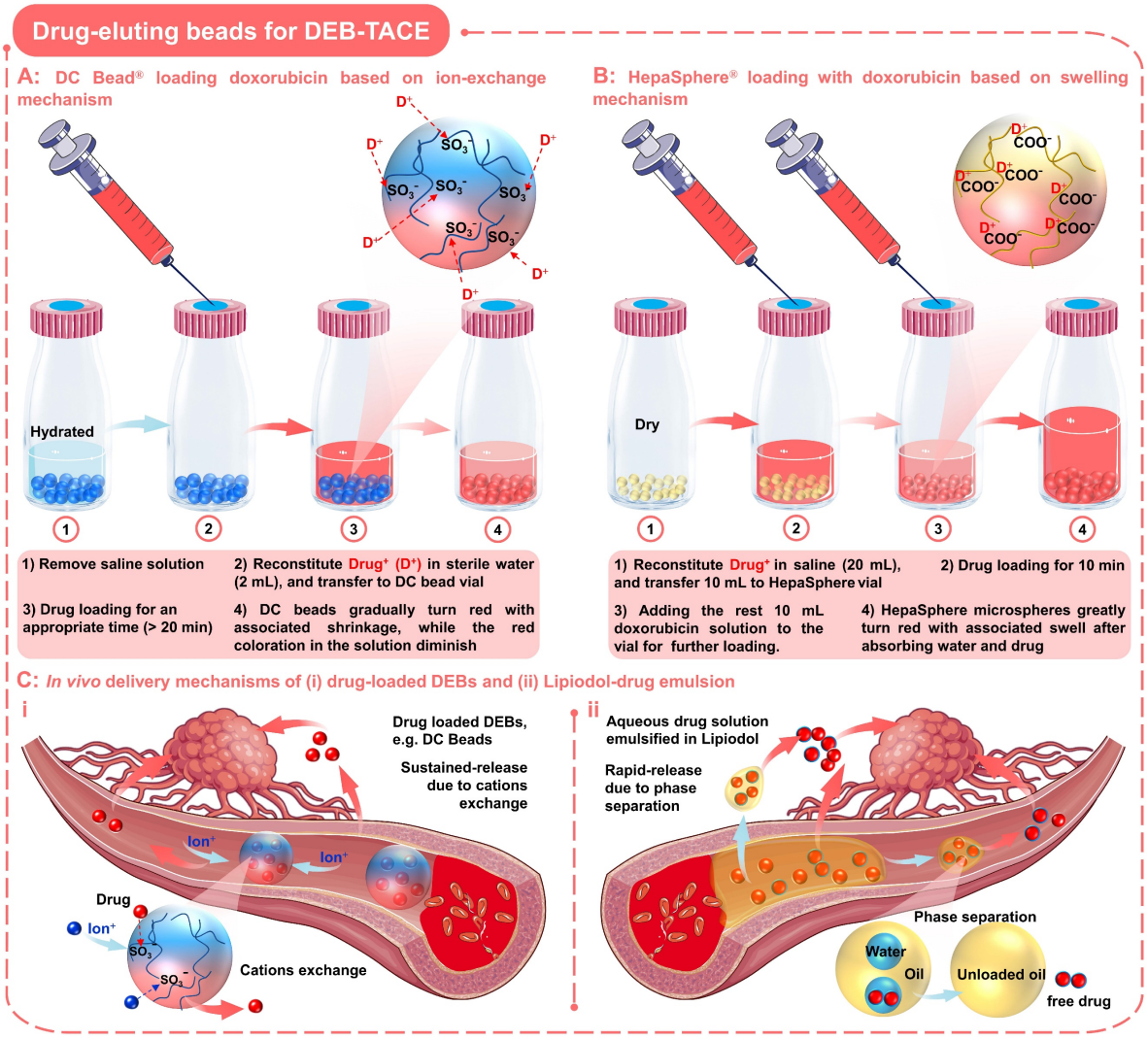

Figure 4. Drug–eluting beads for DEB–TACE. Schematic diagram of drug loading process and mechanism of two commonly used DEBs: (A) DC Bead loading with doxorubicin based on ion–exchange mechanism; (B) HepaSphere loading with doxorubicin based on swelling mechanism. (C) *In vivo* delivery mechanisms of (i) drug–loaded DEBs and (ii) Lipiodol–drug emulsion. Created with BioRender.com and Smart.Servier.com.

In addition, other DEBs based on swelling mechanisms have also been developed, such as gelatin [86], poly (lacticco–glycolic acid) (PLGA) [87] and alginate [88] based polymeric hydrogels microspheres [89]. These absorbent microspheres seem to be feasible for drug loading, especially for those anionic (e.g., ketoprofen) [86]. Furthermore, the insoluble drugs can also be directly encapsulated into the embolic particles, while the drug release is associated with structure destruction.

2.3 Imageable embolic microspheres

The visualization of embolic agents is critical in interventional therapy, which may facilitate the effective localization of embolic agents, improve therapy control and follow–up assessment, and increase the success rate of TACE. However, conventional embolic microspheres and drug–eluting beads still face the drawback of lacking real–time tracking capabilities, which brings difficulties for physicians to precisely target the treatment area, appropriately detect and standardize end points [90, 91], opportunely identify potential insufficient or non–target embolization [59], thereby compromising clinical safety and outcomes. The visualization capabilities can be obtained by simple physical mixing of the embolic agents with the iodinated contrast media [36, 47]. Unfortunately, the fluidity and diffusibility of the contrast medium may cause systemic toxicity and misdiagnosis [65, 92, 93]. Therefore, there has always been widespread interest in the development of intrinsically imageable embolic microspheres. Initially, researchers aimed to incorporate as many radiopaque components as possible in the embolic microspheres to improve their X–ray imaging capabilities. Later, as medical imaging technology evolved, a wealth of medical diagnostic techniques was applied to TACE. Thus, the focus

shifted to developing multiple imaging materials to render embolic agents more comprehensive imaging modalities. In general, the basic concept remains unchanged, while it is more desirable to find the delicate balance between the need for sufficient imageability and the maintenance of appropriate physicochemical properties [38].

Currently, diverse inclusions (e.g., iodine–containing species, heavy elements, superpara-magnetic substances, and phase–changing materials) have been investigated to impart embolic particle imaging capabilities (Table 2).

Table 2. Selection of imageable embolic microsphere systems described in the literature.

Imaging modality	Embolic matrix	Imaging component	Method of inclusion	Comments	Study (year)	Ref.
X–ray	PHEMA	Iodine (triiodobenzyl groups)	Covalent coupling	25–30 wt% loading	Horak *et al.* (1987)	[94]
X–ray	PMMA (hydrolyzed)	Barium sulfate	Precipitation	70 wt% loading achieved	Thanoo and Jayakrishnan (1989)	[95]
X–ray	PHEMA	Iodine (iothalamic/iopanoic acid)	Covalent esterification	30 wt% loading achieved	Jayakrishnan *et al.* (1990)	[96]
X–ray	PHEMA	Barium sulfate	Entrapment	40–50 wt% loading achieved	Thanoo and Jayakrishnan (1990)	[97]
X–ray	Silicone	Tantalum powder	Entrapment	Needed surface modn.	Thanoo and Jayakrishnan (1991)	[98]
X–ray	PHEMA copolymer	Iodine (triiodobenzyl monomer)	Copolymerization	27 wt% achieved	Horak *et al.* (1997)	[99]
X–ray	PHEMA/PVP copolymers	Iodine (monoiodobenzyl monomer)	Copolymerization	20 wt% achieved	van Hooy–Corstjens *et al.* (2008)	[100]
CT	Alginate	MoS2 nanosheets	Entrapment	12% loading	Fu *et al.* (2017)	[101]
CT	PLGA	Iodine (2,3,5–triiodobenzoic acid (TIBA))	Entrapment	23.15 wt % Iodine loading/Sorafenib loading demonstrated	Choi *et al.* (2017)	[102]
CT	Polystyrene	Tantalum oxide	Entrapment	9.4 wt% tantalum oxide loading	Morrison *et al.* (2015)	[103]
CT	PLAU	Iodine (4,4′ –isopropylidinedi–(2,6–diiodophenol) (IBPA))	Copolymerization	14.48 wt% Iodine loading	Sang *et al.* (2017)	[72]
CT	PVAL	Iodine (4–iodobenzyl or 2,3,5–triiodobenzyl groups)	Copolymerization	40–70 wt % Iodine loading	Agusti *et al.* (2015)	[104]
MR	Trisacryl (Embosphere)	Iron oxide (SPIO)	Entrapment	Detectable by common echo sequences	Namur *et al.* (2007)	[105]
MR	Trisacryl (Embosphere)	Iron oxide (SPIO)	Entrapment	100% detectable	Lee *et al.* (2008)	[106]
MR	PVA	Gadolinium III Chelates	Covalent coupling	45.5 µg Gd(III)/mg PVA	Cilliers *et al.* (2008)	[107]
MR	Chitosan	Iron oxide (SPIO)	Entrapment	1.0 mM SPIO loading	Chung *et al.* (2012)	[108]
MR	Alginate	Prohance® and Holmium ions	Complexation/entrapment	T1 MRI & T2 MRI 0~1.35wt% Ho^{3+} loading	Van *et al.* (2015)	[109]
MR	Alginate	Iron oxide (SPIO)	Entrapment	0.06 ~ 6.0 mg/mL SPIO loading	Wang *et al.* (2017)	[67]
MR/gamma	Alginate	Holmium	Complexation	1.3 wt% Ho loading	Zielhuis *et al.* (2007)	[110]
CBCT/MR	Alginate	Holmium and iodine (Lipiodol)	Complexation/entrapment	0.38% Ho loading	Oerlmans *et al.* (2015)	[111]
DSA/CT	Alginate	Barium sulfate	Complexation	Microfluidic method	Wang *et al.* (2015) Du *et al.* (2018)	[88, 112]
DSA/CT	Alginate	Tantalum nanoparticles	Entrapment	10 w/v% Ta loading	Zeng *et al.* (2018)	[93]
DSA/CT/MRI	P(MAOETIB–GMA)	Iodine/ Iron oxide (SPIO)	Copolymerization/ Precipitation	diameter 40–200 µm	Bartling *et al.* (2011)	[113]
Radiography/MR/CT	PMAA (Embozene)	Barium sulfate/iodine/iron oxide	Precipitation/entrapment	Three different loading densities	Stampfl *et al.* (2012)	[114]
Fluoro/µCT/CT	PVA–AMPS (DC/LC bead)	Iodine (Lipiodol)	Entrapment	Dose–dependent imaging	Sharma *et al.* (2010)	[115]
Fluoro/µCT/CT	PVA–AMPS (DC/LC bead)	Iodine (Lipiodol)	Entrapment	Correlation with drug	Dreher *et al.* (2012)	[116]
Fluoro/µCT/MDCT/CBCT	PVA–AMPS (DC/LC bead)	Iodine (Lipiodol)	Entrapment	Different imaging modes	Tacher *et al.* (2016)	[117]
µCT/CT	PVA–AMPS (DC/LC bead)	Iodine (triiodobenzyl groups)	Covalent attachment	Drug loading demonstrated	Negussie *et al.* (2015)	[118]
Fluoro/µCT/CT	PVA–AMPS (DC/LC bead)	Iodine (triiodobenzyl groups)	Covalent attachment	IR imaging reading study	Duran *et al.* (2016)	[119]
US/MR/PA	PLGA	SPIO/Perfluorohexane	Entrapment	double–emulsion process	You *et al.* (2016)	[120]

Note: CBCT: Cone–beam computed tomography; CT: Computed tomography; DSA: Digital subtraction angiography; Ho: Holmium; modn: Modification; MDCT: Multidetector computed tomography; MR: Magnetic resonance; PHEMA: Poly(2–hydroxyethyl methacrylate); PLAU: Poly(lactic acid)–polyurethane; PLGA: poly(lactic–co–glycolic acid); P(MAOETIB–GMA): homopolymerization of 2–methacryloy–loxyethyl (2,3,5–triiodobenzoate) (MAOETIB) with glycidyl methacrylate (GMA). PMMA: Poly(methylmethacrylate); PVP: Poly(N–vinyl–2–Pyrrolidone); PMAA: Poly(methylacrylic acid); PVA–AMPS: Poly(vinyl alcohol–co–2–acrylamido–2–methylpropane sulfonate); SPIO: Super paramagnetic iron oxide; US: Ultrasound; PA: Photoacoustic. Expanding based on the work of Lewis et al. [38]

2.3.1 X–ray Visible embolic microspheres

X–ray-based imaging (including fluoroscopy (i.e., digital radiography), computed tomography (CT), and digital subtraction angiography (DSA)) has shown significant advantages due to high diagnosis efficiency, high image resolution, and accurate diagnosis results [121]. In general, elements with high atomic numbers and atomic mass all have the potential to absorb X–rays. Therefore, radiopaque properties are often imparted by introducing materials with high densities, such as organoiodine, metals, metal oxides, and metal compounds (Figure 5 and Figure 6A).

The incorporation of organoiodine compounds (such as iodine species containing iodinated benzyl groups (Figure 5A‑C and Figure 6A, i) has been widely studied for the introduction of intrinsic radiopacity into polymeric microspheres [38]. The major approaches include a) copolymerization (Figure 5A) of radiopaque monomers with embolic matrix, b) chemical attachment (Figure 5B) of radiopaque moiety on the prefabricated particles, and c) entrapment (Figure 5C, no bonding) of iodine‑containing compounds within the host particle structure [102, 104, 119]. The first two approaches provide synthetic flexibility and allow the incorporation of high iodine content (even as high as 70%, Table 2) to improve radiopacity. The chemical reaction will bring a certain degree of adverse effects on the necessary properties (e.g., hydrophilicity, softness, smoothness, flexibility, uniformity, and dispersibility) [38]. However, if the iodine content is appropriately balanced (25~30wt%), these microspheres can still effectively embolize the hepatic arteries and maintain fine visibility. Besides, it is worth noting that there are some commercially available radiopaque drug–eluting beads (e.g., LC Bead LUMI™, DC Bead LUMI™, and X–Spheres) have overcome some of these issues (Table 3) [73, 122]. Moreover, the radiopaque microspheres can also be prepared by loading commercial X–ray contrast agents (e.g., Lipiodol), benefiting from the absorbent properties of dry microspheres (as illustrated schematically in Figure 5C) [62]. These Lipiodol–loaded beads show intrinsic radiopacity, superior embolization ability (sufficient embolization, adjustable embolization diameter, and less ectopic embolism compared to pure Lipiodol) [38], and maintain sustained drug release characteristics [116]. However, since no bond is formed, it is important that the organoiodine compounds remain entrapped and do not overflow over time [38]. In general, the incorporation of organoiodine compounds is a practical and efficient approach to impart inherent radiopacity and will show broad prospects in future clinical evaluation.

Table 3. Summary of commercially available imageable beads [38, 73, 74].

Feature	LC Bead LUMI™	DC Bead LUMI™	X–Spheres®
Company	BTG	BTG	Interface Biomaterials
Imaging modality	X–ray	X–ray	X–ray
Material	Triiodobenzyl (TIB)–modified acrylamido–polyvinylalcohol–AMPS hydrogel microspheres	TIB–modified acrylamido–polyvinylalcohol–AMPS hydrogel microspheres	TIB–modified acrylic microspheres
Size (μm)	70–150, 100–300	70–150, 100–300	400–600, 600–710, 710–850
Inclusion method	Covalently bounding of iodine moiety (TIB) into the PVA hydrogel structure	Directly coupling of TIB groups to the 1,3–diol units of the beads	Polymerization of methacrylate monomer that contains covalently bound iodine–derivative
Time to market	Cleared by the US FDA in December 2016	CE marked in March 2017	First authorized in 2015
Labeled indication	Hypervascular tumors and arteriovenous malformations (AVMs)	Nonmalignant hypervascular tumors and AVMs	

FDA: Food and Drug Administration; CE: Communate Europpene.

To satisfy the precise imaging requirement, another innovative strategy is proposed to incorporate functional nanomaterials into microspheres to form a 'nano–in–micro' (or called 'nano–on–micro') system (Figure 5D and Figure 6A, ii) [71, 123]. There are two major approaches: a) encapsulation and b) *in situ* generation. For most metal nanoparticles or metal oxide particles that are difficult to synthesize (such as Ta (Figure 6A, ii) [93] and TaO_x (Figure 6A, iii) [103] nanoparticles), they can be encapsulated into the embolic matrix. For some nanoparticles that can be synthesized by precipitation or redox reactions (such as $BaSO_4$ (Figure 6A, iv) [88, 112], Bi_2S_3 [124], Au (Figure 6A, ii) [125]), they can be *in situ* generated within the embolic structure.

As a typical example, microfluidic technology can be conveniently used to realize 'nano–in–micro' structured alginate embolic microspheres, since alginate can quickly cross–link with metal ions to form a hydrogel (Figure 5D and Figure 6A, ii–iv). For example, Yang's group applied a one–step electrospraying method (Figure 5D, ii) to synthesize tantalum nanoparticles (Ta NPs) loaded calcium alginate microspheres (Ta@CaAlg) (Figure 6A, ii), by spraying a mixture of Ta NPs and sodium alginate into $CaCl_2$ solution [93]. In this study, renal embolization was performed in rabbits using optimized Ta@CaAlg microspheres (330 μm, containing 10 wt% Ta NPs). And the relative X–ray signal intensity was 6490, which is comparable to that of Iodixanol solution (7355). Besides, the *in vivo* results showed that Ta@CaAlg microspheres possessed both embolic and contrast agent properties. Compared with radiolucent calcium alginate microspheres (without tantalum), Ta@CaAlg microspheres were visible in

both digital radiography and CT scans 4 weeks after embolization, indicating the potential for real–time imaging and long–term assessment. Similarly, Yang's group also used the electrospraying method (Figure 5D, ii) to fabricate barium alginate microspheres loaded with *in situ* synthesized $BaSO_4$ particles ($BaSO_4$@BaAlg microspheres) (Figure 6A, iv), by spraying a mixed solution (sodium alginate and Na_2SO_4 mixture) into the collecting bath ($BaCl_2$ solution) [88]. Monodispersed $BaSO_4$@BaAlg microspheres with sizes ranging from 200 to 1800 μm could be achieved by varying the electrospray parameters. While the X–ray visibility was demonstrated through *in vitro* test (CT values: 7 wt % $BaSO_4$, 2172 ± 164 HU Vs. Iohexol solution containing 300 mg iodine (I) mL^{-1}, 3703 ± 153 HU), and the radiodensity remained stable for over 52 days. Through routine renal artery embolization, the embolic effect and intrinsic radiopacity of the $BaSO_4$@BaAlg microspheres were confirmed. However, more studies on the *in vivo* distribution and metabolism mechanisms are needed to better understand how these chemically stable and water–insoluble inclusions are cleared.

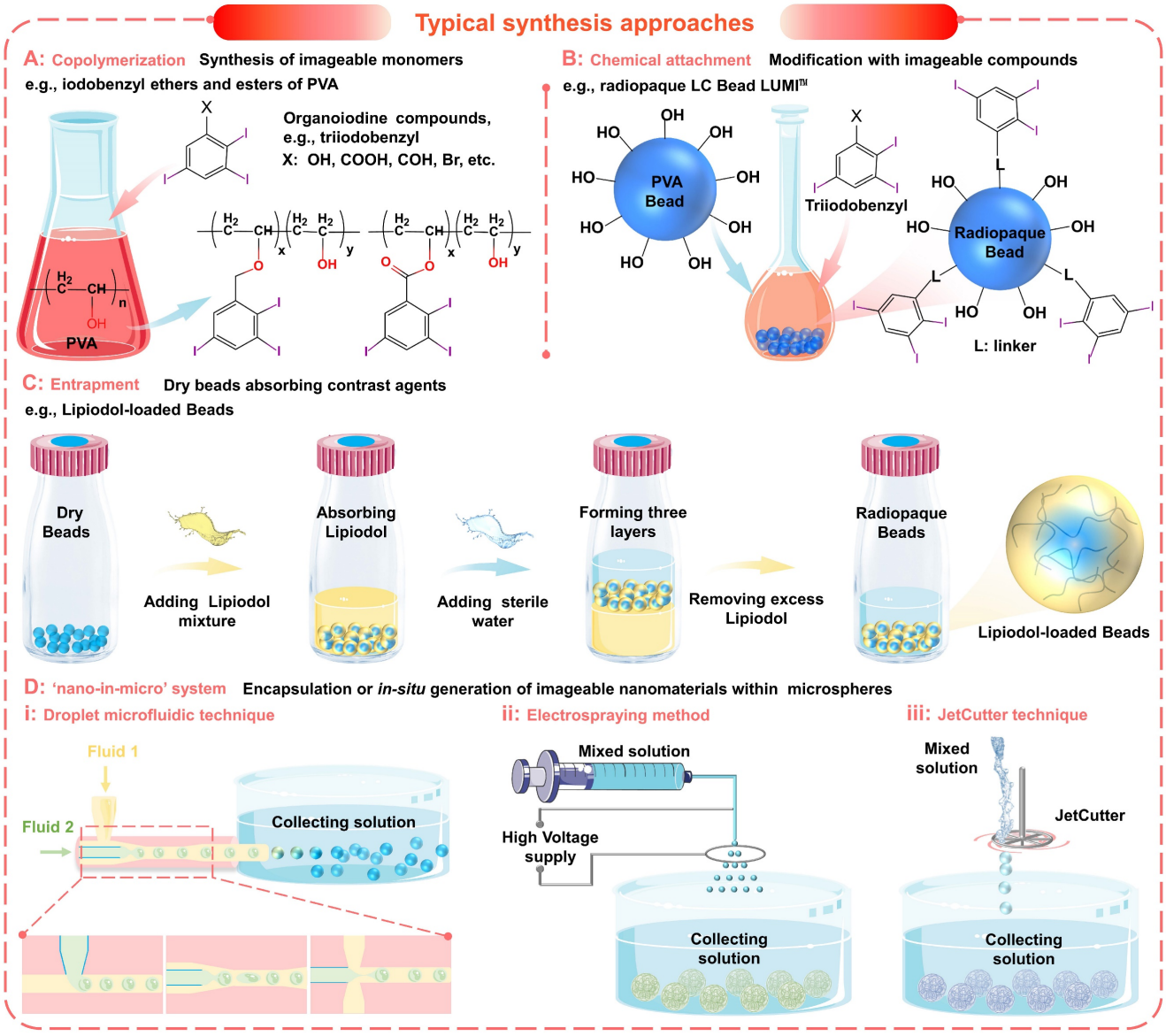

Figure 5. Typical synthesis approaches of imageable embolic microspheres. (A) Synthesis of imageable monomers by copolymerization, e.g., iodobenzyl ethers and esters of poly (vinyl alcohol) (PVA). (B) Chemical attachment of imageable compounds onto the prefabricated particles, e.g., radiopaque LC Bead LUMI™. (C) Entrapment of contrast agents within the host particle structure, e.g., Lipiodol–loaded Beads. (D) Encapsulation or *in situ* generation of imageable nanomaterials within microspheres to form a 'nano–in–micro' (or called 'nano–on–micro') system: (i) droplet microfluidic technique; (ii) electrospraying method; (iii) JetCutter technique.

2.3.2 MRI Visible embolic microspheres

Recently, magnetic resonance imaging (MRI) has also received extensive attention in TACE therapy, considering no ionizing radiation, multi-azimuth imaging, plentiful diagnostic information, high resolution for soft tissue, and 3D visualization/ localization [123, 126-128]. With these benefits, there is a great incentive to transition to MRI–guided interventional therapy. Currently, some examples of real–time MRI applications are routinely performed or will be available in the near future, such as real–time MRI guided cardiovascular interventional therapy [128-131], thermal ablation [132], cryoablation [133-136], and radiotherapy [137, 138], etc. While MRI technologies continue to evolve, perhaps the most pressing focus is on translation to clinical TACE.

MRI technology is a clinical imaging modality that measures the nuclear magnetic resonance (NMR) signals emitted by protons in human bodies under a magnetic field [139]. There are two types of MRI contrast agents that can significantly improve MRI performance by affecting the MR signal properties of the surrounding tissues [140]. a) T_1–weighted contrast agents (or positive contrast agents), which can shorten the longitudinal relaxation times (T_1) of protons, leading to brighter images in T_1–weighted MRI; b) T_2–weighted contrast agents (or negative contrast agents), which can shorten the transverse relaxation times (T_2) of protons, resulting in darker images in T_2–weighted MRI. Currently, most commercially available MRI contrast agents are T_1–weighted contrast agents based on gadolinium (Gd) chelates (Figure 6B, i) [139, 140]. However, the U.S. Food and Drug Administration (FDA) has recommended a prohibition in all patients with acute renal insufficiency [141], due to the Gd–associated nephrotoxicity [139]. Therefore, MRI contrast agents based on magnetic iron oxide nanoparticles (MIONs) have received increasing attention because of their superior biocompatibility and safety (iron is an essential element in the human body) (Figure 6B, i) [139]. In general, superparamagnetic iron oxide nanoparticles (SPIO NPs) are commonly served as T_2–weighted contrast agents, such as FDA approved Feraheme (vascular imaging) and Feridex I.V. (liver and spleen imaging) [142]. But the dark images caused by T_2–weighted contrast agents may be confused with signals from other pathogens, thus affecting the diagnosis. Fortunately, extremely small MIONs (ES–MIONs, smaller than 5 nm) have recently emerged as potential positive contrast agents (Figure 6B, i) [139].

Previously, there have been sporadic attempts to combine Gd (III) chelate with embolic microspheres to realize MRI visualization. For instance, Cilliers et al. modified the Gd (III) chelate on the surface of commercial PVA particles (Contour®, diameter 45–150 μm) with Gd (III) content of 45.5 μg/mg (chemical attachment: Figure 5B and Figure 6B, ii) [107]. After modification, the T_1 relaxation times decreased by more than 80 %, from 1200 ms to 225 ms. In another study, van Elk et al. encapsulated temperature–sensitive liposomes (loaded Gd (III) chelate) into hydrogel microspheres (325 μm), to monitor drug release and microgel deposition (JetCutter technique: Figure 5D, iii) [109]. After mild hyperthermia, the Gd (III) chelates were almost completely released and the T_1–weighted MRI signal intensity increased more than 3 times. Although these studies indicated that the Gd (III) chelates were marginally released or controllable released *in vitro*, they still cannot eliminate the possibility of nephrotoxicity since these chelates may form strong complexes with biological ligands *in vivo* [143, 144]. Therefore, the development of MIONs–based embolic microspheres with better biocompatibility has rekindled the interest of scholars [67, 123, 145-148]. For example, Li et al. synthesized SPIONs–loaded polymeric microspheres (SPMs, 100–300, 300–500 500–700, 700–900 μm) by inverse suspension polymerization method (Figure 6B, iii) [147]. Due to the size limitation, SPMs can only be applied to negative contrast enhancement of T_2–weighted MRI, which is difficult to correctly display the position and distribution of microspheres *in vivo*. In contrast, Wang et al. prepared PVA hybrid microspheres with dual–modal MRI imageability, in which *in situ* synthesized Gd_2O_3 and Fe_3O_4 nanoparticles act as T_1 and T_2–weighted MRI contrast agents, respectively (droplet microfluidic technique: Figure 5D, i and Figure 6B, iv) [123]. This is a compromise approach to obtain T_1/T_2–weighted MRI imageability, and perhaps embolic microspheres based entirely on MIONs and ES–MIONs will be developed in the near future. Overall, although X–ray-based imaging is the dominant technology for real–time monitoring during the current TACE procedure, the MRI–guided TACE under development will show advantages in the future [149].

2.3.3 Multimodal Visible embolic microspheres

In addition, the embolic microspheres that integrated multimodal imaging capabilities may cope with the needs of different diagnostic scenarios and provide more comprehensive information. The most universal and practical strategy is to incorporate materials with different imaging capabilities into the embolic matrix (Figure 6C). Years ago, H. Bartling et al. proposed the formation of multimodal–visible embolic macroparticles (diameter, 40–200 μm) by

suspension homopolymerization of glycidyl methacrylate with 2–methacryloyloxyethyl (2,3,5–triiodobenzoate), which consist of X–ray visible iodine–containing core and MRI–visible Fe_3O_4 particles coating (150 nm) (Figure 6C, i) [113]. The *in vivo* renal embolization revealed that at least partial devascularization was achieved, thus confirming the embolic efficiency. And the signal changes caused by these particles were found in the three imaging modalities (DSA, CT, and MRI), which contribute to monitoring the *in vivo* localization and distribution of the particles. Besides, Stampfl et al. modified commercial Embozene microspheres (polyphosphazene–coated poly (methyl methacrylate), Boston Scientific, Marlborough, MA, USA) by impregnation of iodine and precipitation of barium sulfate and iron oxide, to achieve multimodal imaging visibility for radiography, MR imaging, and CT (Figure 6C, ii) [114]. Moreover, hydrated holmium–Lipiodol–alginate microspheres (Ho–lip–ams, 570 ± 12 μm) were prepared by cross–linking alginate–oil emulsion (1:1, alginate: oil, w/w) with chloride salt of holmium ($HoCl_3$, 25mM) (JetCutter technique: Figure 5D, iii and Figure 6C, iii) [111]. Within the microspheres, the inclusion of Lipiodol offered visualization capabilities for fluoroscopy and CT, while the holmium ions (0.38 ± 0.01% (w/w)) allowed MR imaging. When incubated in fetal calf serum (FCS) at 37 °C, these microspheres remained intact, but Lipiodol was gradually released for two weeks. When these microspheres were injected into the organ, a similar deposition pattern was also observed in different imaging modalities. Additionally, Kim et al. demonstrated that the inclusion of radiopaque gold nanorods and magnetic iron clusters in the alginate microspheres could also achieve MRI/CT dual–modality visualization (Figure 6C, iv) [150]. As an alternative CT contrast agent, gold NPs may improve the limitations of conventional iodine contrast agents [151]. In short, utilizing complementary characteristics of X–ray-based imaging and MRI, the TACE procedure can be optimized (guiding intra– and post–procedural visualization, preventing ectopic embolization, accurately determining the endpoint of embolization, and improving follow–up examinations) [111, 113]. However, it will undoubtedly increase the complexity of the embolic system and raise concerns about stability, toxicity, and biocompatibility, despite the feasibility of the incorporation method. Thus, researchers should also consider reasonable trade–offs between complex embolic systems and multiple multimodal imaging capabilities.

2.4 Microspheres for radioembolization

Historically, radiotherapy has played an important role in cancer treatment, which is independent of chemical therapy or other energy–based ablation techniques [152]. Due to the radiosensitive nature of normal hepatic tissue (< 30 Gy [153]), tumoricidal radiation dose (> 70 Gy [154]) to solid liver tumors will lead to severe complications (including liver failure and other fatal gastrointestinal symptoms [155]), which limits the application in HCC. Thus, selective delivery of radioactive embolic microspheres into the tumor arterial is essential for safe and successful radiotherapy in hepatic malignancies [152]. Consequently, the concept of transarterial radioembolization (TARE, or as selective internal radiation therapy (SIRT)) was introduced, which is a combination of brachytherapy and embolization using the same technical principle as cTACE [15, 156].

The therapeutic effect of TARE is mainly exerted by the carried radiation source rather than the chemical or ischemic effect (Figure 7A–B), for which microspheres loaded with Yttrium–90 (^{90}Y) are commonly used [156]. Yttrium–90 is a pure β emitter with a short half–life (64.2 h) and limited tissue penetration (average 2.5 mm, maximum 11 mm) [156], which allows local high–dose radiation while minimizing the risk of radiation–induced normal hepatic necrosis (Figure 7C). There are two types of commercially available ^{90}Y microspheres for treating hepatic neoplasms, namely 1) TheraSphere® (BTG International, London, United Kingdom) and 2) SirSpheres® (Sirtex Medical Europe, Bonn, G) [152, 156]. All other radioactive microspheres are either investigational or not clinical, such as ^{166}Ho and ^{188}Re–based microspheres [157, 158]. TheraSphere® is composed of nonbiodegradable glass, in which ^{90}Y radioisotope act as an integral constituent of the glass matrix.

Table 4. Characteristics and differences of commercially available ^{90}Y–particles [152, 156].

Feature	TheraSphere®	SIR–Spheres®
Isotope	90Y	90Y
Half-life (h)	64.2	64.2
Material	Glass	Resin
Diameter (μm)	20–30	20–60
Activity per particle (Bq)	2500	50
Spheres per 3 GBq	1.2×10^6	$40–80 \times 10^6$
Activity in the vial (GBq)	3, 5, 7, 10, 15, or 20 %	3% ± 10%
Number of microspheres (vial, million)	1.2–8	40–80
Specific Gravity (g/mL)	3.2	1.6
Embolic effect	Negligible	Mild
Contrast injection	No	During infusion
FDA approved indication	Unresectable HCC	CRC liver metastases with intrahepatic floxuridine

FDA: Food and Drug Administration; CRC: Colorectal cancer; HCC: Hepatocellular carcinoma.

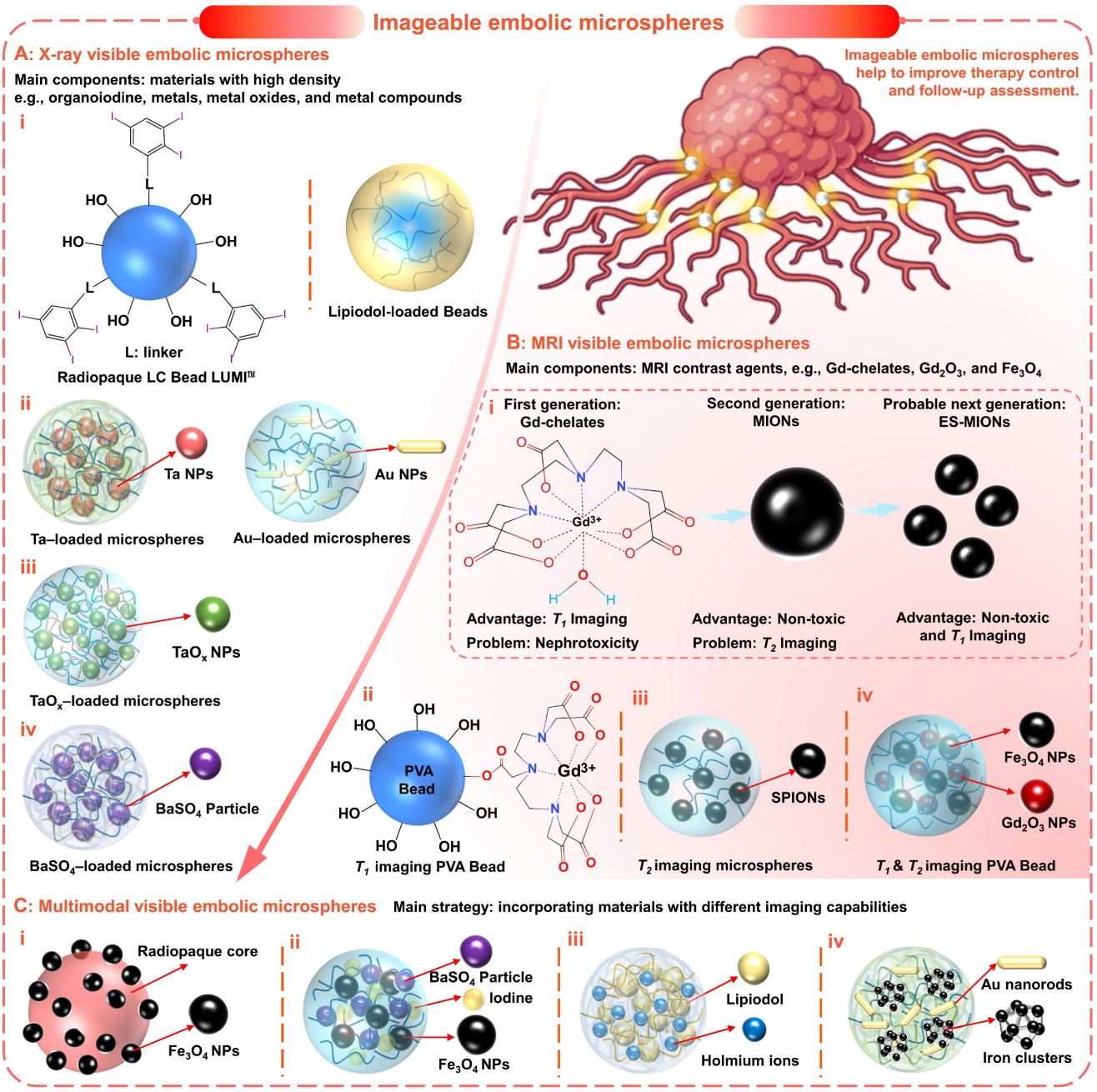

Figure 6. Imageable embolic microspheres help to improve therapy control and follow–up assessment. (A) Typical X–ray visible embolic microspheres based on radiopaque materials, such as (i) organoiodine (e.g., triiodobenzyl, Lipiodol), (ii) metals (e.g., tantalum (Ta), gold (Au)), (iii) metal oxides (e.g., TaO_x), and (iv) metal compounds (e.g., $BaSO_4$). (B) Typical MRI visible embolic microspheres based on MRI contrast agents: (i) main problems and advantages of current and future MRI contrast agents, e.g., T_1–weighted contrast agents (gadolinium (Gd) chelate), T_2–weighted contrast agents (magnetic iron oxide nanoparticles, MIONs), and T_1–weighted contrast agents (extremely small MIONs, ES–MIONs, smaller than 5 nm); (ii) PVA Bead modified with Gd (III) chelates for T_1 imaging; (iii) superparamagnetic iron oxide nanoparticles (SPIONs, ~12nm) loaded polymerized microspheres for T_2 imaging; (iv) PVA hybrid microspheres loaded with Gd_2O_3 and Fe_3O_4 nanoparticles (~5 nm) for T_1 & T_2 imaging. (C) Multimodal (X–ray and MRI) visible embolic microspheres were realized by incorporating materials with different imaging capabilities: (i) macroparticle consist of iodine–containing core and Fe_3O_4 particles coating; (ii) Embozene microspheres modified with iodine impregnation and $BaSO_4$/Fe_3O_4 precipitation; (iii) hydrated alginate microspheres loaded with holmium and Lipiodol; (iv) alginate microspheres containing radiopaque gold nanorods and magnetic iron clusters. Created with BioRender.com.

And it was approved in 1999 for radiotherapy or as neoadjuvant therapy before transplantation, suitable for patients with unresectable HCC in whom the hepatic arterial catheters can be appropriately positioned. Besides, SirSpheres® consists of biodegradable resin–based microspheres with ^{90}Y radioisotopes attached to the surface. And it received premarket approval in 2002 for the treatment of patients with colorectal liver metastases (CRLM) in conjunction with intrahepatic Floxuridine. Other features of these two microspheres, such as specific gravity, radioactivity, and radiation dose, were detailed in Table 4. These different features could explain the differences in hypothetical applications, administration modes, and activity dose for each patient [156], but there were no significant differences

in clinical efficacy [159]. In early clinical trials, the TARE was only used as a salvage option after the failure of first–line therapy [152]. However, the subsequent phase I and phase II clinical investigation [160] and several retrospective studies [15, 161, 162] have revealed the safety and efficacy of TARE using ^{90}Y isotope–loaded particles in the treatment of HCC. Specifically, the HCC patients treated with TARE showed similar therapy responses compared to alternative therapies including cTACE, TACE, and chemotherapy (sorafenib) [163-166]. In general, TARE is becoming a promising treatment option for unresectable primary or secondary liver malignancies [152, 167].

2.5 Microspheres for Arterial Embolization Hyperthermia

Generally, as a palliative treatment, TACE cannot eliminate viable tumor cells, which may result in the failure of TACE due to local tumor recurrence and distant metastasis [120, 170]. For the development and further applications of the TACE, supplemental therapeutic mechanisms, including magnetic induction hyperthermia (MIH) [145, 171], microwave ablation (MWA) [172, 173], high–intensity focused ultrasound (HIFU) thermotherapy [120, 170, 174],

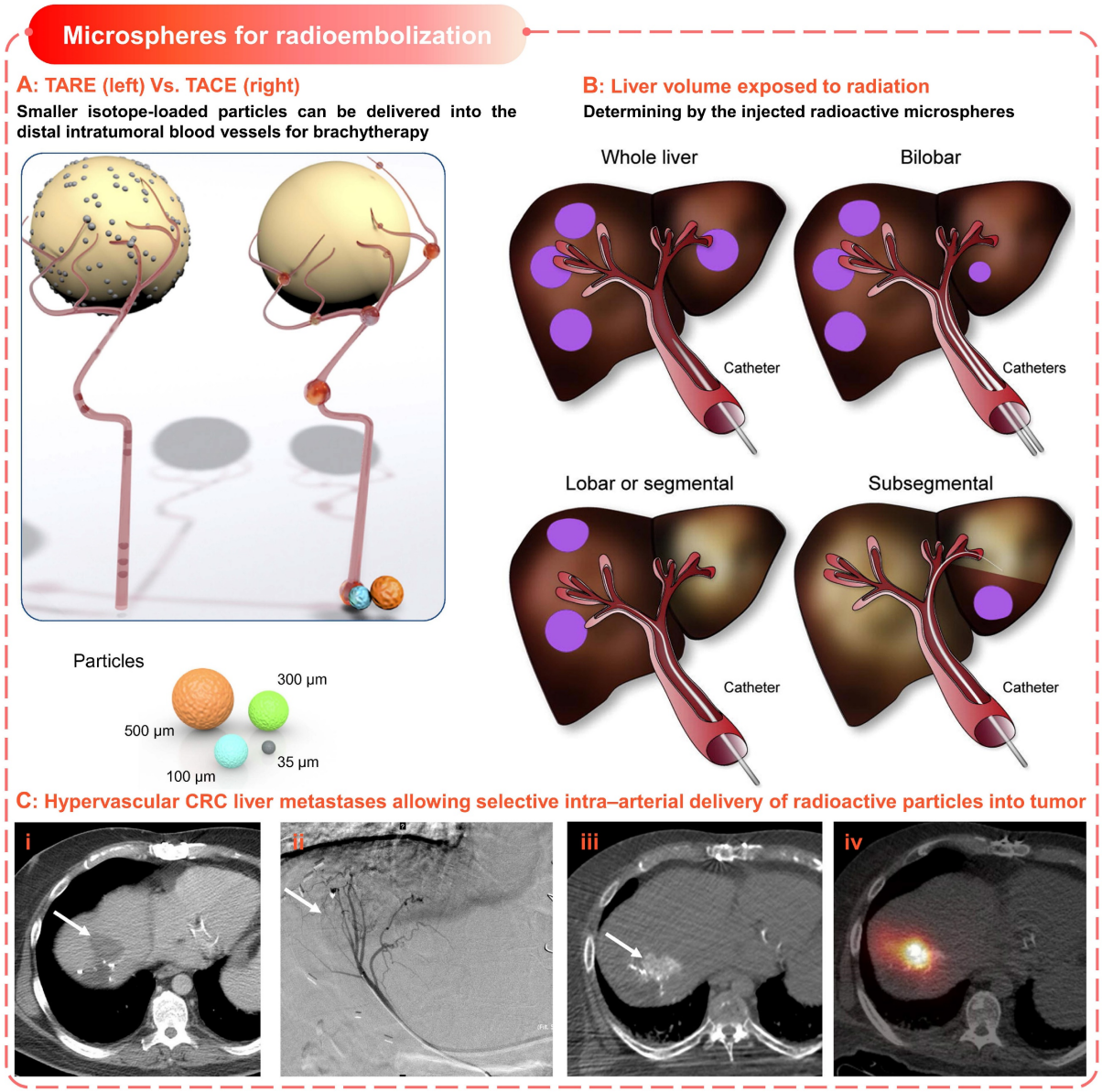

Figure 7. Microspheres for radioembolization. (A) Schematic illustrates the difference of devices and procedures used for TARE and TACE; Smaller isotope–loaded particles can be delivered into the distal intratumoral blood vessels for brachytherapy. Adapted with permission from [168], Copyright 2012 Elsevier. (B) Liver volume exposed to radiation is defined by the injected radioactive microspheres. Adapted with permission from [168], Copyright 2012 Elsevier. (C) Hypervascular colorectal cancer (CRC)liver metastases allowing selective intra–arterial delivery of radioactive particles into the tumor. (i) CRC liver metastases (arrow), (ii) catheter angiogram shows arterial blood supply, (iii) hypervascularity of lesion, (iv) bremsstrahlung SPECT/CT after injection of ^{90}Y microspheres. Adapted with permission from [169], Copyright 2017 Society of Nuclear Medicine.

photothermal therapy (PTT) [175, 176], and radiofrequency ablation (RFA) [177, 178], etc., have been introduced to enhance the therapeutic effects. Extensive clinical studies have confirmed improved outcomes through combination therapy of TACE with interventional thermal/nonthermal ablation modalities [14, 179-181]. In addition to the sequential implementation approaches, the use of stimulus–responsive embolic agents is also a feasible combination method that can enhance the efficacy of targeted hyperthermia, simplify the surgical procedure and minimize the invasiveness. Therefore, the experimental concept of arterial embolization hyperthermia (AEH) has been proposed (Figure 8). Its basic principle is to selectively embolize the hepatic tumor supply arteries with stimulus–responsive embolic agents, followed by external stimulation exposure to generate hysteretic heating of the embolized particles and hence the surrounding tissues [182]. For this purpose, micro/nano materials that are sensitive to external energy fields are often incorporated into the embolic matrices, such as magnetic–sensitive nanoparticles [171], microwave–sensitive nanosheets [101], HIFU–sensitive nanocapsules [120], photothermal–sensitive nanostars [125], and radiofrequency–sensitive nanoclusters [183], etc. Besides, it can also realize active drug release *via* external energy regulation, which will enable a more flexible dosing regimen. Moreover, it is worth mentioning that supplemental thermotherapy can effectively enhance the tumoricidal effects of TAE/TACE, while intravascular embolization can also promote the local accumulation of heat, thus is hopeful to develop a mutually reinforcing treatment model.

2.5.1 Magnetic embolic microspheres

Magnetic embolization hyperthermia is a branch of magnetic targeted hyperthermia, that utilizes magnetic particles to achieve selective arterial embolization and heat generation (magnetic hysteresis loss effects or Neel relaxation under alternating magnetic field (AMF)) [184]. For magnetic embolization hyperthermia, iron and superparamagnetic iron oxide nanoparticles (SPIO NPs) are the main components of the magnetic induction mediator within embolic microspheres. Because they possess a set of required properties, e.g., non–toxic, non–immunogenic, biocompatible, biodegradable, high magnetization saturation, and radiopacity [185]. For instance: Liang et al. fabricated poly (lactic–co–glycolic acid) (PLGA)–magnetic microspheres (MMs, controllable size 100 to 1000 μm) embedded with Fe_3O_4 NPs (20 nm) by a rotating membrane emulsification system (Figure 8A) [171]. And, the MMs were successfully employed for combining TAE and magnetic ablation (TAEMA) to treat orthotopic VX2 liver tumors–bearing rabbits. In this study, the designed magnetic field and microsphere parameters (number, size) can directly adjust the required temperature rise, thereby leading to tumor cell apoptosis (42~46 °C, hyperthermia) or necrosis (>50 °C, ablation). The *in vitro* and *in vivo* results showed that the tumor edge could be heated to more than 15 °C within 30 min when exposed to AMF (390 kHz, 12 A or 500 kHz, 16 A) after TAE, while the temperature increase near the normal liver parenchyma was negligible (< 5 °C). Besides, the phase transition of PLGA (from glass state to rubber state) was also observed when heated to the glass transition temperature (Tg, 50 °C), which may cause adhesion and aggregation to enhance the embolic effect. Theirs follow–up research confirmed that the MMs could effectively load drugs (drug loading coefficient of 8.1 %, and encapsulation efficiency of 94.6 %), and also revealed that the temperature plays a decisive role in drug release [186]. In addition, the simulation and experimental studies of Qiu et al. have shown that the magnetic embolic microspheres can be controllably aggregated in the presence of a magnetic field, showing the potential for the magnetic field–controlled embolization [145]. Compared to direct injection hyperthermia (DIH) with magnetic fluid perfusion (uneven distribution and poor retention in the tumor tissue), magnetic embolization hyperthermia can achieve durable and repeatable targeted magnetic hyperthermia [182]. And several studies have confirmed its preliminary feasibility and efficacy in animal models [182, 187-191].

Simply put, magnetic embolization hyperthermia is a typical paradigm for combining targeted hyperthermia with TAE or TACE, providing a feasible synergistic treatment strategy. However, it is worth considering that long–term exposure to high–intensity AMF may cause patient discomfort, although the application of AMF with frequencies of 0.05–1.5 MHz is a safe method to minimize the impact on healthy tissues.

2.5.2 HIFU–sensitive embolic particles

High–intensity focused ultrasound (HIFU) hyperthermia is an extracorporeal and non–invasive technique that induces coagulative necrosis by thermal injury and mechanical stress [120, 192]. Its combination with TACE is another experimental technique undergoing preclinical evaluation in addition to magnetic embolization hyperthermia [170, 184]. Since several retrospective studies have demonstrated that the combination therapy of TACE plus HIFU ablation was more beneficial than

monotherapy (e.g., TACE, chemotherapy) in different patients with HCC (e.g., children, adults, and elderly; with primary, unresectable, or metastatic liver cancer), which could improve the prognosis and prolong the life expectancy without increasing the incidence of adverse reactions [174, 193-195].

Recently, there have been several studies on HIFU–sensitive micro/nano materials for HIFU embolization hyperthermia. For instance, You et al. explored the HIFU–sensitive composite nanocapsules (Fe_3O_4–PFH/PLGA) with SPIO NPs–integrated PLGA capsules and phase–changing agents (perfluorohexane (PFH)) core by a double–emulsion process, which can be used for the synergistic treatment of TACE plus HIFU ablation (Figure 8B) [120]. During the *in vivo* experiment, the TACE was performed on the VX2 liver tumor–bearing rabbits *via* transarterial injection of a mixture of Fe_3O_4–PFH/PLGA and Lipiodol emulsion, and the HIFU ablation was implemented (0.8 MHz, focal lengths 135 to 155 mm, power 180 W, and exposure duration 5 s) after TACE. In particular, the accumulation and retention of micro/nanocapsules within the targeted areas were enhanced by the TACE, thereby increasing the energy deposition and enlarging the tumor coagulation volume. Besides, the bubbles were generated due to the temperature–induced phase transformation of the PFH core, which further strengthen the embolization and HIFU ablation effects. In addition, this micro/nano system can be applied for ultrasound, magnetic resonance, and photoacoustic tri–modality imaging due to the integration of several functional materials, which is beneficial to assist tumor localization and prognostic diagnosis. Although many questions remain to be verified, such as whether the freely moving bubbles will cause ectopic embolization, it is undeniable that this innovative research may stimulate broad interest in the development of HIFU–sensitive embolic agents.

2.5.3 Microwave sensitive embolic microspheres

Microwave ablation (MWA) utilizes electromagnetic energy to induce tumor coagulative necrosis, which offers the advantages of short delivery time, and a large/predictable ablation zone [14]. Early studies have examined its safety and efficiency as an effective treatment for liver cancer [172, 173, 196]. And several randomized controlled trials (RCT) have demonstrated that the combination therapy of TACE plus MWA is more effective than TACE monotherapy, in respect to higher tumor necrosis rate, better tumor response, longer tumor progression time, and lower complication rate [197-199].

In recent years, microwave (MW)–sensitive micro/nano materials have been developed for MW embolization hyperthermia, which can synergistically maximize tumor necrosis by the targeted hyperthermia and the reduced blood flow "cooling" effect. For example, Meng's group prepared MW–sensitive embolic microspheres by embedding molybdenum sulfide nanosheets within alginate microspheres (MSMCs, 5.6 ± 1.8 μm) (Figure 8C, i) [101]. In the *in vivo* experiments, the MSMCs were injected into the VX2 liver tumor–bearing rabbits *via* a transcatheter arterial route, achieving well distribution in the marginal and internal regions of the tumors. Under MW irradiation, the temperature at the tumor site rapidly increased to 50 °C within 1 min and reached approximately 60 °C within 5 min. Such high and persistent hyperthermia could cause protein denaturation to completely kill cancer cells. Besides, after 3 days of treatment, the ablation zone was observed to be 5 times larger than that of the MWA alone. Thus, this study validated that the combination therapy of MWA and TAE/TACE relying on MW–sensitive embolic microspheres is a promising option for large tumors. In addition, Meng's group also developed chemical drugs and MW–susceptible ionic liquids loaded micro/nanocapsules (Figure 8C, ii) [200]. The heat generation mechanism of ionic liquids may be associated with MW electromagnetism–induced ion movement, molecular arrangement, and charged ion shift [121, 201-203]. Under MW irradiation, the microcapsular structure could be decomposed owing to the increased temperature, leading to the active release of drugs [200]. However, current MWA requires the cooperation of percutaneous puncture technology, and non–invasive methods are still not practicable for treating large and deep tumors due to energy dissipation.

2.5.4 Photothermal sensitive embolic microspheres

Photothermal therapy (PTT) has attracted extensive attention due to its unique advantages including minimal invasiveness, and high specificity, which achieves tumoricidal effects *via* converting light energy (a high–frequency electromagnetic radiation) into heat. However, the current PTT is restricted by the limitations of low tissue penetration, since the laser rapidly attenuates with increasing tissue depth. Although researchers have explored near–infrared (NIR) laser (650 – 950 nm) with high physiological transmissivity and photothermal–sensitive micro/nano materials with enhanced photothermal conversion efficiency, interventional PTT is still needed for deep–seated tumors. For example, laser–induced interstitial thermotherapy (LITT) that utilizes flexible optical fibers to generate cytotoxic temperature within deeply buried tumors, is frequently used after TACE to improve the therapeutic effect of

large–sized HCC. Like other combination therapy, the TACE plus LITT also showed better tumor regression [175] and significantly longer overall survival than monotherapy of LITT [204] or TACE [205].

In order to further improve the therapeutic effect and simplify the repeated embolization step, the development of photothermal–sensitive embolic microspheres is meaningful. The basic strategy is similar to other stimulation–susceptible embolic agents introduced earlier, that is, the inclusion of photothermal conversion agents (such as gold [125], iron oxide [206], and bismuth [124, 207] based nanoparticles) into the embolic matrix (Figure 8D). For example, Huang et al. synthesized photothermal–sensitive composite microspheres by an inverse emulsion copolymerization, in which polydopamine coated SPIO NPs (SPION@PDA) and doxorubicin were encapsulated (Figure 8D, i) [206]. Although satisfactory tumor responses (tumor size decreased by 91.5 %) were achieved with the combination treatment of TACE plus PTT in VX2 liver tumor–bearing rabbits, the supplemental therapeutic mechanism of PTT still required laparotomy to expose the hepatic tumor, which is a bit superfluous. In short, compared to other non–invasive hyperthermia modalities, pure material innovation is only the "icing on the cake" for the combination therapy of TACE plus PTT, while there is still a long way to go.

2.5.5 Radiofrequency sensitive embolic agents

Radiofrequency ablation (RFA) as a valuable treatment for unresectable HCC [178] has been widely considered as the gold standard therapy treatment in combination with TAE/TACE [179]. During the RFA, the friction heat can be generated in targeted tumor sites *via* ionic agitation, owing to the high–frequency alternating currents launched from needle–electrodes (directly inserted into tumor nodules) [208]. However, the RFA of irregularly shaped tumors is still challenging since the friction heat losses rapidly in the hypervascular tumor regions. Similarly, TAE/TACE has been used synergistically with RFA to reduce the blood flow "cooling" effect in the ablation zone, and superior therapeutic outcomes were found in clinical practice [209, 210].

Recently, several radiofrequency (RF) sensitive embolic agents have been applied to coordinate the antitumor efficacy of TAE/TACE and RFA [183, 211]. For example, Li et al. synthesized RF–sensitive embolic agents (dvGC@PNAs), in which the temperature–sensitive poly (N–isopropylamide–co–acrylic acid) (PNAs) was modified onto RF–sensitive dual–valent gold nanoclusters (dvGC) *via* gold–sulfur coordination bond (Figure 8E, i) [183]. Vascular embolization can be achieved when the dvGC@PNAs were infused into the tumor arteries, attributing to temperature–sensitive sol–gel transition of PNAs (maintain flowability at room temperature and convert to high gelation strength at body temperature). When RFA therapy was administered at 3 d post–TAE operation, the dvGC@PNAs mediated the synergistic effect of TAE and RFA was realized due to the RF–induced heating effect of dvGC. More importantly, they substantiated that the tumor microenvironment post–TAE procedure was greatly improved, ascribing to a favorable immune response induced by the RF–responsive dvGC@ PNAs. In their subsequent research, the cisplatin–crosslinking PNAs nanogels (Pt–PNAs) were further developed as RF–responsive embolic nano–platform *via* the coordination bonding between Pt (II) ions and carboxyl (Figure 8E, ii), which could be used for improving the synergistic effect of TACE and RFA [211]. In the future, it may be possible to realize a more efficient combination therapy of TAE/TACE and RFA, relying on RF–responsive material innovation. However, the invasive treatment model of RFA remains an insurmountable challenge.

3. Multifunctional fully flexible embolic agents

As previously mentioned, the performance of embolic microspheres is decisive for the improvement of TACE. Currently, the fundamental embolic function and drug–loading/releasing properties are associated with the embolic matrix, while the enhanced functionalities are derived from the additional components. However, simply increasing the variety of additives with beneficial functions will undoubtedly increase the complexity of the embolic system. In addition, most inclusions are rigid and insoluble inorganic materials, that generally lack surface modification (especially those formed *in situ*). Once the encapsulated microspheres are broken or degraded, the naked rigid inclusions will be released and exposed to the complex ionic microenvironment, causing hidden dangers in systemic circulation. Specifically, there may be less intracellular uptake due to the lack of receptor–ligand interaction [212, 213] and more aggregation due to high surface energy [214, 215], leading to potential adverse effects (e.g., prolonged circulation and metabolism, and increased potential for complications). Therefore, gallium (Ga) based liquid metals (LMs) with amorphous properties (superb fluidity, shape transformability, excellent flexibility, low viscosity, and self–healing capability) and inherently diverse functions (good biocompatibility, biodegradability, and facile functionalization accessibility) have aroused widespread interest in the TACE [216-219].

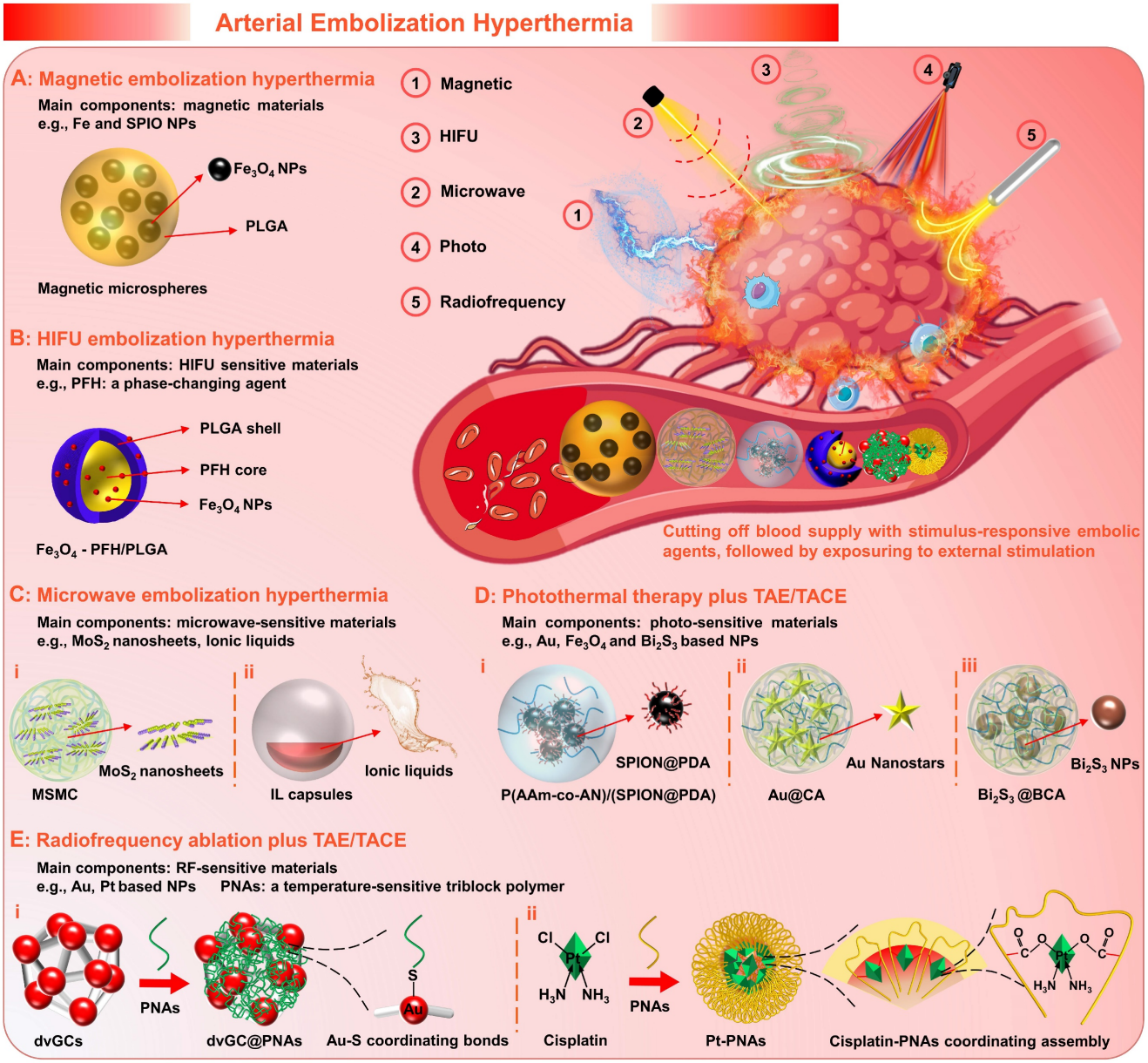

Figure 8. Arterial embolization hyperthermia is hopeful to develop a complementary treatment model, which can not only introduce supplemental therapeutic mechanisms for TACE therapy, but also reduce the blood flow "cooling" effect for hyperthermia (schematic illustration). (A) Magnetic embolization hyperthermia based on magnetic microspheres, e.g., poly (lactic–co–glycolic acid)(PLGA)–magnetic microspheres. (B) High–intensity focused ultrasound (HIFU) sensitive micro/nano materials for HIFU embolization hyperthermia, e.g., Fe_3O_4 nanoparticles–integrated PLGA capsules with phase–changing agents (perfluorohexane (PFH)) core (Fe_3O_4–PFH/PLGA). (C) Microwave (MW) sensitive micro/nano materials for MW embolization hyperthermia, e.g., (i) alginate microspheres embedded with molybdenum sulfide nanosheets (MSMC), (ii) MW susceptible ionic liquids (IL) loaded micro/nanocapsules. (D) Photo–sensitive micro/nano materials for TAE/TACE plus photothermal therapy (PTT), e.g., (i) poly(acrylamide–co–acrylonitrile) microspheres encapsulated with polydopamine coated superparamagnetic iron oxide nanoparticles (P(AAm–co–AN)/(SPION@PDA)), (ii) calcium alginate (CA) hydrogel microspheres containing Au nanostars (Au@CA), (iii) alginate microspheres encapsulated with bismuth sulfide nanoparticles (Bi_2S_3@BCA). (E) Radiofrequency (RF) sensitive embolic agents for coordinating TAE/TACE and radiofrequency ablation, e.g., (i) RF–sensitive dual–valent gold nanoclusters (dvGC) modified with temperature–sensitive poly (N–isopropylamide–co–acrylic acid) (PNAs), (ii) cisplatin–crosslinking PNA nanogels (Pt–PNAs). Created with BioRender.com.

Meaningfully, our united team has revealed that Ga–based LMs offer broad prospects in the field of angiography and intravascular embolization [220-224]. Primary, angiography is of great significance for TACE, since vascular visualization can help to diagnose and evaluate physiological conditions related to blood vessels. With inherent softness, high density, and electromagnetic properties, the LMs can serve as effective medical imaging contrast agents for X–rays [220], CT [220], and MRI [223]. Particularly, when the LMs infused into the vessels, mega contrast X–ray images (Figure 9A) [220] and CT images (Figure 9B) [221] could be generated for multiscale vasculature mapping with high radiographic densities (several orders of higher resolution than that of the Iohexol) and increased penetration depth (visualize

small capillaries, ~100 μm). And the LMs also showed negative T2–weighted MRI contrast enhancement at the vascular embolism site (Figure 9C) [223]. Besides, the LMs functional materials that are sensitive to external energy fields (e.g., magnetic–responsive [223], photo–responsive [225], microwave–responsive [203], ultrasonic–responsive [226], and electrochemical–responsive [227], Figure 9) could also provide supplemental therapeutic functions to TACE without the need of redundant additives. After preliminary verification of the possibility of the macroscopic LMs in vascular embolization (Figure 9D, i) [221], the macroscopic LMs as non–magnetic magnetocaloric sensitizers were also applied for magnetic embolization hyperthermia (Figure 9D, ii) [223]. However, the toxicity and the degradability of the macroscopic LMs should be further evaluated systematically. After that, the LMs particles (~ 1 μm) were further combined with alginate hydrogel for vascular embolization (Figure 9E) [222]. Yet, such *in situ* cross–linked LMs–gel embolic agents could only apply to superficial endovascular embolization. In order to meet clinical needs, our group first explored the soft magnetic LMs nanocomposites for the construction of "nano–in–micro" embolic microspheres, which can be used as multifunctional fully flexible embolic microspheres for dual–modality imaging guided and NIR laser enhanced TACE (Figure 9F) [224]. In particular, these LMs–based microspheres were successfully employed for CT and MR dual–modality imaging, which can not only meet the X–ray radiopacity requirements of current clinical TACE, but also show potential in future MRI–guided TACE to avoid X–ray radioactive hazards. And their paramagnetism also shows potential for magnetic targetability. In addition, their photothermal and photodynamic susceptibility are beneficial for photothermal conversion, ROS generation, and controllable drug release, showing the synergistic antitumor effect of TACE and photothermal/photodynamic therapy. Most importantly, such microspheres were successfully applied for the standard TACE procedures on a domestic pig and a New Zealand white rabbit.

To sum up, different from conventional rigid micro/nano materials, inherently functional LMs will show unique compatibilities in intravascular treatment, providing a facile and versatile strategy to extend the pool of multifunctional fully flexible embolic materials. Theoretically, diverse flexible embolic materials with multiple imaging modes and supplemental therapeutic functions are readily available through the combinatorics of LMs micro–nanomaterials and matrix materials, promising for researchers to explore in the field of TACE.

4. Future Outlooks

As surveyed above, numerous desirable properties of particulate embolic agents have been identified and described in this review. It can be found that due to the intervention of micro/nano technology, the embolic devices have replaced complexity with simplicity while integrating more complete functionality, which will greatly simplify the TACE procedure and improve therapeutic efficiency.

An overview of the current development route and future trends is as follows (Figure 10): 1) The first–generation TACE embolic agents: a mixture of Lipiodol, drugs, and microspheres [15, 19, 36-39]; 2) The second–generation TACE embolic agents: Lipiodol and drug–eluting beads [62]. The use of DEBs significantly improved the drug delivery system, which is a mature first step to incorporating drug loading and releasing functions into the clinical TACE procedures [60, 63]. 3) The third–generation TACE embolic agents: imageable drug–eluting beads [38]. The imageable embolic particles that are foreseeable towards clinical TACE can offer a more precise and controlled procedure than the current use of iodide contrast agents. A typical example is commercially available radiopaque drug–eluting beads (DC Bead LUMI™), which can provide inherent long–term radiopacity as well as the reliable performance of DC Bead [122]. As for whether the multi–mode imageable embolic particles can be used in clinical practice, it depends on the development of medical imaging technology in the TACE procedure. 4) The new generation of TACE embolic agents: multifunctional integrated drug–eluting beads [224]. Although the development of these multifunctional embolic microspheres is still in the early stages, it is undeniable that these essential properties play an essential role. For instance, stimulus sensitivity (e.g., magnetic–responsive [223], photo–responsive [225], microwave–responsive [203], ultrasonic–responsive [226], and electrochemical–responsive [227]) is a reliable way to actively control drug concentration and provide adjuvant therapy. Considering the various cellular and molecular factors involved in the progression of HCC, monotherapy may not be beneficial, especially for large tumors [21]. Fortunately, extensive clinical studies have supported improved outcomes of the combination therapy of TACE and various interventional thermal/nonthermal ablation modalities [14, 179-181]. In the future, the combination of TACE and non–invasive hyperthermia (e.g., MIH [145, 171], MWA) [172, 173], HIFU thermotherapy [120, 170, 174], and PTT [175, 176]) may become an important direction, because of inherent complementary characteristics.

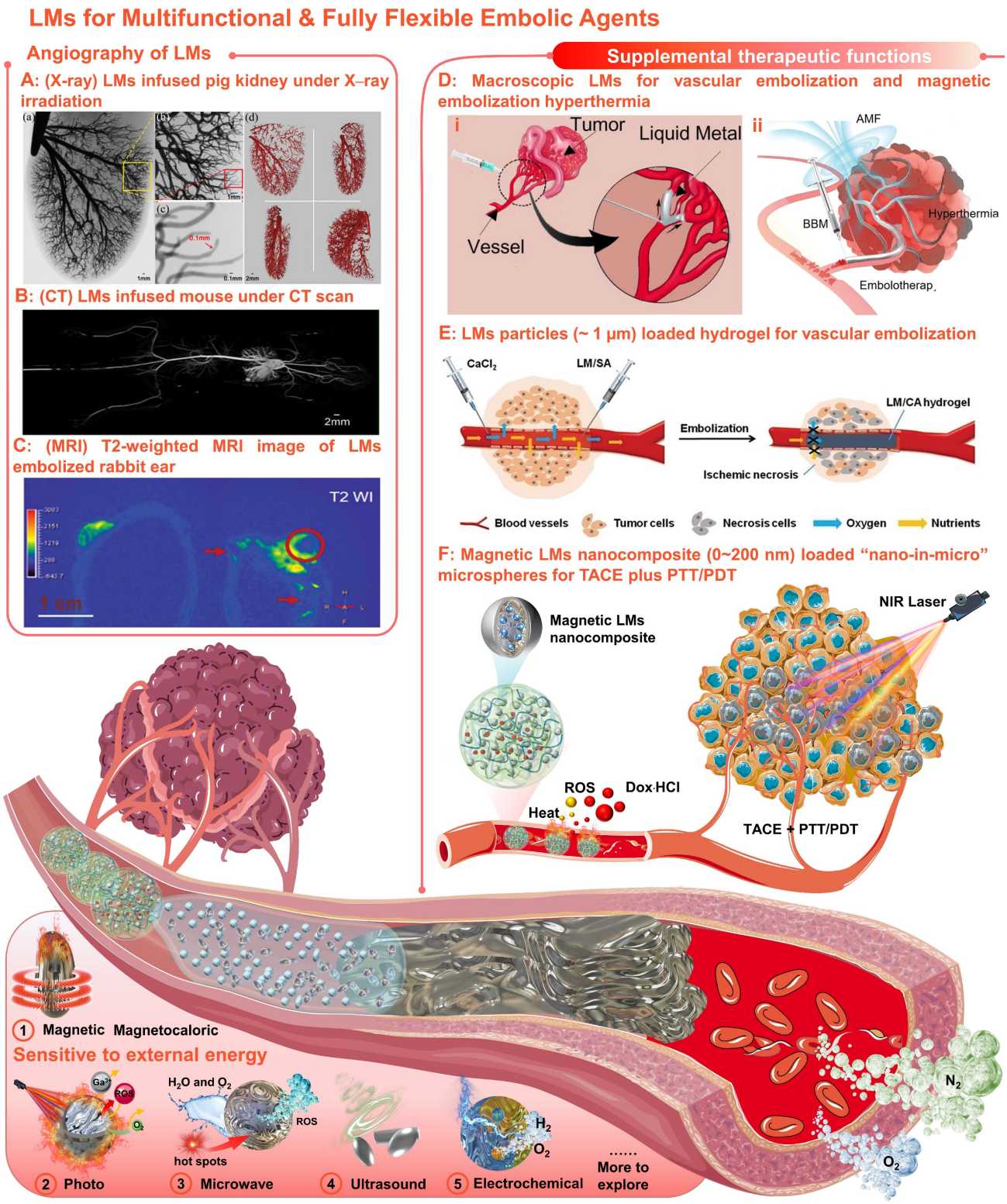

Figure 9. With inherent softness, high density, electromagnetic properties, and sensitivities to external energy fields, LMs could be used as multifunctional & fully flexible embolic agents with no size limitations or redundant additives requirements. (A) Mega contrast vasculature of a pig kidney infused with LMs (Ga) under X–ray irradiation. Adapted with permission from [220], Copyright 2014 IEEE–INST. (B) The CT images of mouse vessels filled with LMs (Ga). Adapted with permission from [221], Copyright 2014 Wang et al. (C) T_2–weighted MRI image of (left) the tumor–bearing rabbit ear and (right) the LMs embolized rabbit ear; The red circle indicated the embolized tumors and the red arrows indicated vessels embolized with LMs (mixture of $Bi_{35}In_{48.6}Sn_{15.9}Zn_{0.4}$ and $Ga_{67}In_{20.5}Sn_{12.5}$). Adapted with permission from [223], Copyright 2022 Wiley–VCH. (D) Macroscopic LMs for (i) vascular embolization (adapted with permission from [221], Copyright 2014 Wang et al. and (ii) magnetic embolization hyperthermia (adapted with permission from [223], Copyright 2022 Wiley–VCH). (E) The LMs particles (~ 1 μm) combined with alginate hydrogel for vascular embolization. Adapted with permission from [222], Copyright 2019 Wiley–VCH. (F) Soft magnetic LMs nanocomposite (0~200 nm) loaded "nano–in–micro" microspheres for TACE plus photothermal and photodynamic therapy (PTT/PDT). Reproduced with permission from [224], Copyright 2021 The Royal Society of Chemistry. Created in Smart.Servier.com.

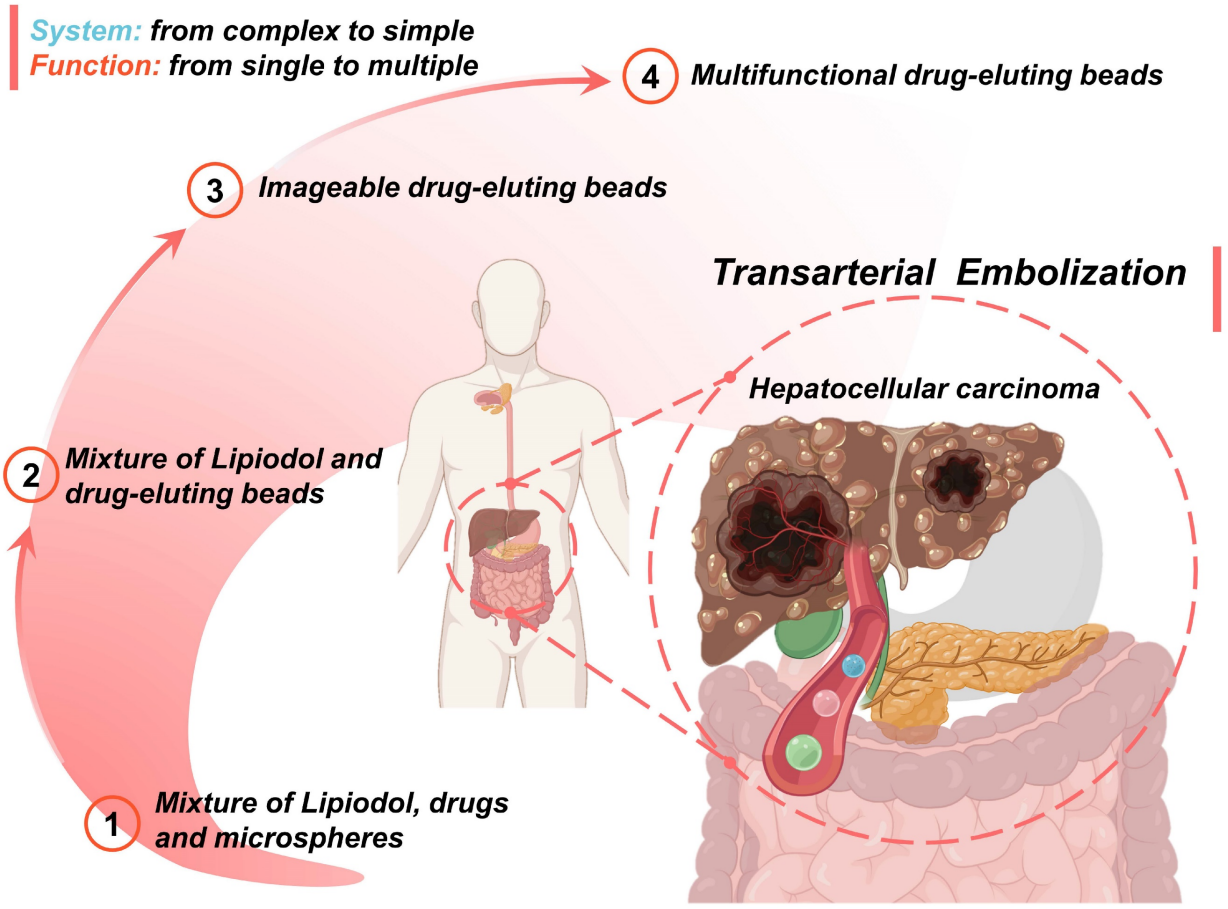

Figure 10. Schematic illustration of the current development routes and future trends of micro/nano embolic agents in transarterial embolization for hepatocellular carcinoma. Created with BioRender.com.

Besides, these ablative modalities can also stimulate an antitumor immune response by locally releasing tumor antigens, however, tumoricidal effects are usually suppressed by the immunosuppressive tumor microenvironment of HCC (immunosuppressive mechanisms involving impaired tumor–associated antigen–processing and presentation, lack of $CD4^+$ T–cell responses, enhanced myeloid–derived suppressor cells, enhanced regulatory T cells, and increased expression of programmed cell death ligand–1 [21]). After receiving neoadjuvant TACE, the ablative modalities in conjunction with antigen–presenting cells (e.g., dendritic cells), or cytotoxic cells (e.g., cytokine–induced killer cells), may offer a potential strategy to augment tumoricidal effects *via* counteracting the immunosuppressive mechanisms of HCC [179]. Another essential function is controllable localization, considering that the current embolic microspheres localized mainly depends on the superselective insertion of the microcatheter and the size–dependent accumulation. In this regard, magnetic embolic agents have shown the preliminary possibility of controllable embolic localization [171, 224]. Moreover, other noteworthy particulate embolic agents that may have an impact on future TACE treatment include LMs micro/nano materials, thrombin encapsulated micro/nano materials [228], and radioactive microspheres (for non–thermal combination therapy, e.g., TACE plus radiation Therapy [156]). Furthermore, the TACE as a necrosis–inducing treatment may unmask tumor rejection of antigen–mediated immunity, thus providing a rationale for combining TACE with immunotherapy [229].

To sum up, the use of functional micro/nano materials to obtain ideal multifunctional particulate embolic agents may not be far from reality and may lead to a more comprehensive treatment method. However, for the intravascular application of these micro/nano materials, long–term research on the biodistribution, toxicity, and biocompatibility in the human body is required, and standard surgical procedures also need to be studied.

5. Conclusions

In summary, this review systematically identified and described recently emerging micro/nano materials as particulate embolic agents, with

emphasis on materials, typical features, various functions, and practical applications. Particularly, new insights into the liquid metals–based multifunctional and flexible embolic agents were highlighted, which may have a broader impact on future angiography and intravascular embolization. Besides, the current development routes and future outlooks of these emerging micro/nano embolic materials were also concluded. Overall, the development of next-generation embolic agents with properties such as degradability, drug–loading and releasing properties, detectability, targetability, and multiple therapeutic modalities is crucial for the improvement of TACE. This review provides an in-depth understanding of newly developed micro/nano embolic agents, which may inspire multidisciplinary researchers to collaboratively innovate the next generation of embolic agents.

Acknowledgements

This work was financially supported by the National Key R&D Program of China (2018YFC1 705106) and the National Natural Science Foundation of China (No. 51890893).

Competing Interests

The authors have declared that no competing interest exists.

References

1. Siegel RL, Miller KD, Jemal A. Cancer statistics, 2020. CA Cancer J Clin. 2020; 70: 7-30.
2. Forner A, Reig M, Bruix J. Hepatocellular carcinoma. The Lancet. 2018; 391: 1301-14.
3. Sung H, Ferlay J, Siegel RL, Laversanne M, Soerjomataram I, Jemal A, et al. Global cancer statistics 2020: Globocan estimates of incidence and mortality worldwide for 36 cancers in 185 countries. CA Cancer J Clin. 2021; 71: 209-49.
4. Meza-Junco J, Montano-Loza AJ, Liu DM, Sawyer MB, Bain VG, Ma M, et al. Locoregional radiological treatment for hepatocellular carcinoma; which, when and how? Cancer Treat Rev. 2012; 38: 54.
5. Pitton MB, Kloeckner R, Ruckes C, Wirth GM, Eichhorn W, Worns MA, et al. Randomized comparison of selective internal radiotherapy (SIRT) versus drug-eluting bead transarterial chemoembolization (DEB-TACE) for the treatment of hepatocellular carcinoma. Cardiovasc Intervent Radiol. 2015; 38: 352-60.
6. Lencioni R. Chemoembolization for hepatocellular carcinoma. Semin Oncol. 2012; 39: 503-9.
7. Thomas MB, Jaffe D, Choti MM, Belghiti J, Curley S, Fong Y, et al. Hepatocellular carcinoma: Consensus recommendations of the national cancer institute clinical trials planning meeting. J Clin Oncol. 2010; 28: 3994-4005.
8. Forner A, Gilabert M, Bruix J, Raoul J-L. Treatment of intermediate-stage hepatocellular carcinoma. Nature Reviews Clinical Oncology. 2014; 11: 525-35.
9. Akoad ME, Pomfret EA. Surgical resection and liver transplantation for hepatocellular carcinoma. Clin Liver Dis. 2015; 19: 381-99.
10. Lencioni R, Crocetti L. Local-regional treatment of hepatocellular carcinoma. Radiology. 2012; 262: 43-58.
11. Bruix J, Reig M, Sherman M. Evidence-based diagnosis, staging, and treatment of patients with hepatocellular carcinoma. Gastroenterology. 2016; 150: 835-53.
12. Balogh J, Victor D, 3rd, Asham EH, Burroughs SG, Boktour M, Saharia A, et al. Hepatocellular carcinoma: A review. J Hepatocell Carcinoma. 2016; 3: 41-53.
13. Bruix J, Gores GJ, Mazzaferro V. Hepatocellular carcinoma: Clinical frontiers and perspectives. Gut. 2014; 63: 844-55.
14. O'Leary C, Mahler M, Soulen MC. Liver-directed therapy for hepatocellular carcinoma. Chin Clin Oncol. 2021; 10: 8.
15. Vogl TJ, Gruber-Rouh T. HCC: Transarterial therapies-what the interventional radiologist can offer. Dig Dis Sci. 2019; 64: 959-67.
16. Wang YX, De Baere T, Idee JM, Ballet S. Transcatheter embolization therapy in liver cancer: An update of clinical evidences. Chin J Cancer Res. 2015; 27: 96-121.
17. Li H, Wu F, Duan M, Zhang G. Drug-eluting bead transarterial chemoembolization (TACE) vs conventional TACE in treating hepatocellular carcinoma patients with multiple conventional TACE treatments history: A comparison of efficacy and safety. Medicine. 2019; 98: e15314.
18. Nouri YM, Kim JH, Yoon HK, Ko HK, Shin JH, Gwon DI. Update on transarterial chemoembolization with drug-eluting microspheres for hepatocellular carcinoma. Korean J Radiol. 2019; 20: 34-49.
19. Idee JM, Guiu B. Use of lipiodol as a drug-delivery system for transcatheter arterial chemoembolization of hepatocellular carcinoma: A review. Crit Rev Oncol Hematol. 2013; 88: 530-49.
20. Nishikawa H, Kita R, Kimura T, Osaki Y. Transcatheter arterial embolic therapies for hepatocellular carcinoma: A literature review. Anticancer Res. 2014; 34: 6877-86.
21. Klungboonkrong V, Das D, McLennan G. Molecular mechanisms and targets of therapy for hepatocellular carcinoma. J Vasc Interv Radiol. 2017; 28: 949-55.
22. El-Serag HB, Rudolph KL. Hepatocellular carcinoma: Epidemiology and molecular carcinogenesis. Gastroenterology. 2007; 132: 2557-76.
23. Yan JJ, Liao JZ, Lin JS, He XX. Active radar guides missile to its target: Receptor-based targeted treatment of hepatocellular carcinoma by nanoparticulate systems. Tumour Biol. 2015; 36: 55-67.
24. Folkman J. Role of angiogenesis in tumor growth and metastasis. Semin Oncol. 2002; 29: 15-8.
25. Mellal L, Folio D, Belharet K, Ferreira A. Modeling of optimal targeted therapies using drug-loaded magnetic nanoparticles for liver cancer. IEEE Trans Nanobioscience. 2016; 15: 265-74.
26. Tam KY, Leung KC, Wang YX. Chemoembolization agents for cancer treatment. Eur J Pharm Sci. 2011; 44: 1-10.
27. Riccardo L, Crocetti L. Local-regional treatment of hepatocellular carcinoma. Radiology. 2012; 262: 43-58.
28. Yagublu V, Caliskan N, Lewis AL, Jesenofsky R, Gasimova L, Löhr JM, et al. Treatment of experimental pancreatic cancer by doxorubicin-, mitoxantrone-, and irinotecan-drug eluting beads. Pancreatology. 2013; 13: 79-87.
29. Kim B, Han SW, Choi SE, Yim D, Kim JH, Wyss HM, et al. Monodisperse microshell structured gelatin microparticles for temporary chemoembolization. Biomacromolecules. 2018; 19: 386-91.
30. Breedis C, Young G. The blood supply of neoplasms in the liver. Am J Pathol. 1954; 30: 969.
31. Nakashima T, Kojiro M. Pathologic characteristics of hepatocellular carcinoma. Semin Liver Dis. 1986; 6: 259-66.
32. Liapi E, Geschwind JF. Transcatheter arterial chemoembolization for liver cancer: Is it time to distinguish conventional from drug-eluting chemoembolization? Cardiovasc Intervent Radiol. 2011; 34: 37-49.
33. Vaidya S, Tozer KR, Chen J. An overview of embolic agents. Semin Intervent Radiol. 2008; 25: 204-15.
34. Hu J, Albadawi H, Chong BW, Deipolyi AR, Sheth RA, Khademhosseini A, et al. Advances in biomaterials and technologies for vascular embolization. Adv Mater. 2019; 31: 1901071.
35. Sheth RA, Sabir S, Krishnamurthy S, Avery RK, Zhang YS, Khademhosseini A, et al. Endovascular embolization by transcatheter delivery of particles: Past, present, and future. J Funct Biomater. 2017; 8: 12.
36. Poursaid A, Jensen MM, Huo E, Ghandehari H. Polymeric materials for embolic and chemoembolic applications. J Control Release. 2016; 240: 414-33.
37. Liu Q, Qian Y, Li P, Zhang S, Liu J, Sun X, et al. ^{131}I-labeled copper sulfide-loaded microspheres to treat hepatic tumors via hepatic artery embolization. Theranostics. 2018; 8: 785-99.
38. Lewis AL, Willis SL, Dreher MR, Tang Y, Ashrafi K, Wood BJ, et al. Bench-to-clinic development of imageable drug-eluting embolization beads: Finding the balance. Future Oncol. 2018; 14: 2741-60.
39. Ni JY, Xu LF, Wang WD, Sun HL, Chen YT. Conventional transarterial chemoembolization vs microsphere embolization in hepatocellular carcinoma: A meta-analysis. World J Gastroenterol. 2014; 20: 17206-17.
40. Doucet J, Kiri L, O'Connell K, Kehoe S, Lewandowski RJ, Liu DM, et al. Advances in degradable embolic microspheres: A state of the art review. J Funct Biomater. 2018; 9: 14.
41. Dick R. Radiology now. Therapeutic angiographic embolization. Br J Radiol. 1977; 50: 241.
42. Kunstlinger F, Brunelle F, Chaumont P, Doyon D. Vascular occlusive agents. Am J Roentgenol. 1981; 136: 151-6.
43. Nitta N, Ohta S, Tanaka T, Takazakura R, Nagatani Y, Kono N, et al. Gelatin microspheres: Initial clinical experience for the transcatheter arterial embolization. Eur J Radiol. 2008; 67: 536-40.
44. Yamada R, Nakatsuka H, Nakamura K, Sato M, Itami M, Kobayashi N, et al. Hepatic artery embolization in 32 patients with unresectable hepatoma. Osaka City Med J. 1980; 26: 81-96.
45. Yamada R, Sato M, Kawabata M, Nakatsuka H, Nakamura K, Takashima S. Hepatic artery embolization in 120 patients with unresectable hepatoma. Radiology. 1983; 148: 397-401.
46. Yamashita N, Saitou K, Takagi A, Maruyama A. Preparation and characterization of gelatin sponge millispheres injectable through microcatheters. Medical Devices: Evidence and Research. 2009; 2: 19-25.

47. Barnett BP, Gailloud P. Assessment of embogel--a selectively dissolvable radiopaque hydrogel for embolic applications. J Vasc Interv Radiol. 2011; 22: 203-11.
48. Lazzaro MA, Badruddin A, Zaidat OO, Darkhabani Z, Pandya DJ, Lynch JR. Endovascular embolization of head and neck tumors. Front Neurol. 2011; 2: 64.
49. Makuuchi M, Sukigara M, Mori T, Kobayashi J, Yamazaki S, Hasegawa H, et al. Bile-duct necrosis - complication of transcatheter hepatic arterial embolization. Radiology. 1985; 156: 331-4.
50. Nakamura H, Tanaka T, Hori S, Yoshioka H, Kuroda C, Okamura J, et al. Transcatheter embolization of hepatocellular carcinoma: Assessment of efficacy in cases of resection following embolization. Radiology. 1983; 147: 401-5.
51. Zhang Y, Liu Y. Transcatheter arterial chemoembolization of hepatocellular carcinoma with 350-560 μm gelatin sponge particles: Efficacy, tumour response and survival. Chinese journal of hepatology. 2013; 21: 637-8.
52. Herrera M, Rysavy J, Kotula F, Rusnak B, Castanedazuniga WR, Amplatz K. Ivalon shavings: Technical considerations of a new embolic agent. Radiology. 1982; 144: 638-40.
53. Tadavarthy SM, Knight L, Ovitt TW, Snyder C, Amplatz K. Therapeutic transcatheter arterial embolization. Radiology. 1974; 112: 13-6.
54. Loffroy R, Guiu B, Cercueil JP, Krause D. Endovascular therapeutic embolisation: An overview of occluding agents and their effects on embolised tissues. Curr Vasc Pharmacol. 2009; 7: 250-63.
55. Sun X, Dai H, Guo P, Sha X. Biocompatibility of a new kind of polyvinyl alcohol embolic microspheres: *In vitro* and *in vivo* evaluation. Mol Biotechnol. 2019; 61: 610-21.
56. Kettenbach J, Stadler A, Katzler IV, Schernthaner R, Blum M, Lammer J, et al. Drug-loaded microspheres for the treatment of liver cancer: Review of current results. Cardiovasc Intervent Radiol. 2008; 31: 468-76.
57. Bendszus M, Klein R, Burger R, Warmuth-Metz M, Hofmann E, Solymosi L. Efficacy of trisacryl gelatin microspheres versus polyvinyl alcohol particles in the preoperative embolization of meningiomas. Am J Neuroradiol. 2000; 21: 255-61.
58. Kettenbach J, Stadler A, Iv, Schernthaner R, Blum M, Lammer J, Rand T. Drug-loaded microspheres for the treatment of liver cancer: Review of current results. Cardiovasc Intervent Radiol. 2008; 31: 468-76.
59. Gonsalves CF, Brown DB. Chemoembolization of hepatic malignancy. Abdom Imaging. 2009; 34: 557-65.
60. Song JE, Kim DY. Conventional vs drug-eluting beads transarterial chemoembolization for hepatocellular carcinoma. World J Hepatol. 2017; 9: 808-14.
61. Lammer J, Malagari K, Vogl T, Pilleul F, Denys A, Watkinson A, et al. Prospective randomized study of doxorubicin-eluting-bead embolization in the treatment of hepatocellular carcinoma: Results of the precision v study. Cardiovasc Intervent Radiol. 2010; 33: 41-52.
62. Johnson CG, Tang Y, Beck A, Dreher MR, Woods DL, Negussie AH, et al. Preparation of radiopaque drug-eluting beads for transcatheter chemoembolization. J Vasc Interv Radiol. 2016; 27: 117-26.
63. Ikeda K. Recent advances in medical management of hepatocellular carcinoma. Hepatol Res. 2019; 49: 14-32.
64. Baur J, Ritter C, Germer C-T, Klein I, Kickuth R, Steger U. Transarterial chemoembolization with drug-eluting beads versus conventional transarterial chemoembolization in locally advanced hepatocellular carcinoma. Hepat Med. 2016; 8: 69-74.
65. Lewis AL, Gonzalez MV, Lloyd AW, Hall B, Tang Y, Willis SL, et al. Dc bead: *In vitro* characterization of a drug-delivery device for transarterial chemoembolization. J Vasc Interv Radiol. 2006; 17: 335-42.
66. Boulin M, Guiu S, Chauffert B, Aho S, Cercueil JP, Ghiringhelli F, et al. Screening of anticancer drugs for chemoembolization of hepatocellular carcinoma. Anticancer Drugs. 2011; 22: 741-8.
67. Wang Q, Liu S, Yang F, Gan L, Yang X, Yang Y. Magnetic alginate microspheres detected by MRI fabricated using microfluidic technique and release behavior of encapsulated dual drugs. Int J Nanomedicine. 2017; 12: 4335-47.
68. Ngan B-Y, Forte V, Campisi P. Molecular angiogenic signaling in angiofibromas after embolization: Implications for therapy. Arch Otolaryngol Head Neck Surg. 2008; 134: 1170-6.
69. Virmani S, Rhee TK, Ryu RK, Sato KT, Lewandowski RJ, Mulcahy MF, et al. Comparison of hypoxia-inducible factor-1α expression before and after transcatheter arterial embolization in rabbit VX2 liver tumors. J Vasc Interv Radiol. 2008; 19: 1483-9.
70. Pawlik TM, Reyes DK, Cosgrove D, Kamel IR, Bhagat N, Geschwind JF. Phase ii trial of sorafenib combined with concurrent transarterial chemoembolization with drug-eluting beads for hepatocellular carcinoma. J Clin Oncol. 2011; 29: 3960-7.
71. Bannerman D, Wan W. Multifunctional microbeads for drug delivery in TACE. Expert Opinion on Drug Delivery. 2016; 13: 1289-300.
72. Sang L, Luo D, Wei Z, Qi M. X-ray visible and doxorubicin-loaded beads based on inherently radiopaque poly(lactic acid)-polyurethane for chemoembolization therapy. Mater Sci Eng, C. 2017; 75: 1389-98.
73. Caine M, Carugo D, Zhang X, Hill M, Dreher MR, Lewis AL. Review of the development of methods for characterization of microspheres for use in embolotherapy: Translating bench to cathlab. Adv Healthc Mater. 2017; 6.
74. Pérez-López A, Martín-Sabroso C, Gómez-Lázaro L, Torres-Suárez AI, Aparicio-Blanco J. Embolization therapy with microspheres for the treatment of liver cancer: State-of-the-art of clinical translation. Acta Biomater. 2022; 149: 1-15.
75. Malagari K. Drug-eluting particles in the treatment of HCC: Chemoembolization with doxorubicin-loaded dc bead. Expert Rev Anticancer Ther. 2008; 8: 1643-50.
76. Sadick M, Haas S, Loehr M, Elshwi M, Singer MV, Brade J, et al. Application of dc beads in hepatocellular carcinoma: Clinical and radiological results of a drug delivery device for transcatheter superselective arterial embolization. Onkologie. 2010; 33: 31-7.
77. Dubbelboer IR, Lilienberg E, Ahnfelt E, Sjogren E, Axen N, Lennernas H. Treatment of intermediate stage hepatocellular carcinoma: A review of intrahepatic doxorubicin drug-delivery systems. Ther Deliv. 2014; 5: 447-66.
78. Biondi M, Fusco S, Lewis AL, Netti PA. Investigation of the mechanisms governing doxorubicin and irinotecan release from drug-eluting beads: Mathematical modeling and experimental verification. J Mater Sci Mater Med. 2013; 24: 2359-70.
79. Lewis AL, Dreher MR, O'Byrne V, Grey D, Caine M, Dunn A, et al. Dc bead™: Towards an optimal transcatheter hepatic tumour therapy. J Mater Sci Mater Med. 2016; 27: 13.
80. Wang Y, Molin DG, Sevrin C, Grandfils C, van den Akker NM, Gagliardi M, et al. *In vitro* and *in vivo* evaluation of drug-eluting microspheres designed for transarterial chemoembolization therapy. Int J Pharm. 2016; 503: 150-62.
81. Malagari K, Pomoni A, Filippiadis D, Kelekis D. Chemoembolization of hepatocellular carcinoma with hepasphere™. Hepatic Oncology. 2015; 2: 147-57.
82. de Luis E, Bilbao JI, de Ciercoles JA, Martinez-Cuesta A, de Martino Rodriguez A, Lozano MD. *In vivo* evaluation of a new embolic spherical particle (hepasphere) in a kidney animal model. Cardiovasc Intervent Radiol. 2008; 31: 367-76.
83. Jordan O, Denys A, De Baere T, Boulens N, Doelker E. Comparative study of chemoembolization loadable beads: *In vitro* drug release and physical properties of dc bead and hepasphere loaded with doxorubicin and irinotecan. J Vasc Interv Radiol. 2010; 21: 1084-90.
84. Malagari K, Pomoni M, Moschouris H, Kelekis A, Charokopakis A, Bouma E, et al. Chemoembolization of hepatocellular carcinoma with hepasphere 30-60 μm. Safety and efficacy study. Cardiovasc Intervent Radiol. 2014; 37: 165-75.
85. Zurstrassen CE, Gireli LPO, Tyng CJ, Bitencourt AGV, Guimaraes MD, Barbosa PNV, et al. Safety and efficacy of hepasphere 50-100 μm in the treatment of hepatocellular carcinoma. Minim Invasive Ther Allied Technol. 2017; 26: 212-9.
86. Zhou C, Cui D, Zhang Y, Yuan H, Fan T. Preparation and characterization of ketoprofen-loaded microspheres for embolization. J Mater Sci Mater Med. 2012; 23: 409-18.
87. Lee SY, Choi JW, Lee J-Y, Kim D-D, Kim H-C, Cho H-J. Hyaluronic acid/doxorubicin nanoassembly-releasing microspheres for the transarterial chemoembolization of a liver tumor. Drug Deliv. 2018; 25: 1472-83.
88. Du Q, Li L, Liu Y, Zeng J, Li J, Zheng C, et al. Fabrication of inherently radiopaque $BaSO_4$@BaAlg microspheres by a one-step electrospraying method for embolization. Journal of Materials Chemistry B. 2018; 6: 3522-30.
89. Chen YP, Zhang JL, Zou Y, Wu YL. Recent advances on polymeric beads or hydrogels as embolization agents for improved transcatheter arterial chemoembolization (TACE). Front Chem. 2019; 7: 408.
90. Jin B, Wang D, Lewandowski RJ, Riaz A, Ryu RK, Sato KT, et al. Chemoembolization endpoints: Effect on survival among patients with hepatocellular carcinoma. AJR Am J Roentgenol. 2011; 196: 919-28.
91. Iwazawa J, Ohue S, Hashimoto N, Muramoto O, Mitani T. Survival after c-arm CT-assisted chemoembolization of unresectable hepatocellular carcinoma. Eur J Radiol. 2012; 81: 3985-92.
92. Saralidze K, van Hooy-Corstjens CS, Koole LH, Knetsch ML. New acrylic microspheres for arterial embolization: Combining radiopacity for precise localization with immobilized thrombin to trigger local blood coagulation. Biomaterials. 2007; 28: 2457-64.
93. Zeng J, Li L, Zhang H, Li J, Liu L, Zhou G, et al. Radiopaque and uniform alginate microspheres loaded with tantalum nanoparticles for real-time imaging during transcatheter arterial embolization. Theranostics. 2018; 8: 4591-600.
94. Horák D, Metalová M, Švec F, Drobník J, Kálal J, Borovička M, et al. Hydrogels in endovascular embolization. Iii. Radiopaque spherical particles, their preparation and properties. Biomaterials. 1987; 8: 142-5.
95. Thanoo BC, Jayakrishnan A. Radiopaque hydrogel microspheres. J Microencapsul. 1989; 6: 233-44.
96. Jayakrishnan A, Thanoo BC, Rathinam K, Mohanty M. Preparation and evaluation of radiopaque hydrogel microspheres based on phema/iothalamic acid and phema/iopanoic acid as particulate emboli. 1990; 24: 993-1004.
97. Thanoo BC, Jayakrishnan A. Barium sulphate-loaded p(hema) microspheres as artificial emboli: Preparation and properties. Biomaterials. 1990; 11: 477-81.
98. Thanoo BC, Jayakrishnan A. Tantalum loaded silicone microspheres as particulate emboli. J Microencapsul. 1991; 8: 95-101.
99. Horák D, Metalová M, Rypáček F. New radiopaque polyhema-based hydrogel particles. J Biomed Mater Res. 1997; 34: 183-8.
100. van Hooy-Corstjens CSJ, Saralidze K, Knetsch MLW, Emans PJ, de Haan MW, Magusin PCMM, et al. New intrinsically radiopaque hydrophilic

microspheres for embolization: Synthesis and characterization. Biomacromolecules. 2008; 9: 84-90.
101. Fu C, He F, Tan L, Ren X, Zhang W, Liu T, et al. MoS_2 nanosheets encapsulated in sodium alginate microcapsules as microwave embolization agents for large orthotopic transplantation tumor therapy. Nanoscale. 2017; 9: 14846-53.
102. Choi JW, Park JH, Cho HR, Chung JW, Kim DD, Kim HC, et al. Sorafenib and 2,3,5-triiodobenzoic acid-loaded imageable microspheres for transarterial embolization of a liver tumor. Sci Rep. 2017; 7: 554.
103. Morrison R, Thompson J, Bird L, Hill MA, Townley H. Synthesis and characterization of polystyrene embolization particles doped with tantalum oxide nanoparticles for X-ray contrast. J Mater Sci Mater Med. 2015; 26: 218.
104. Agusti G, Jordan O, Andersen G, Doelker É, Chevalier Y. Radiopaque iodinated ethers of poly(vinyl iodobenzyl ether)s: Synthesis and evaluation for endovascular embolization. J Appl Polym Sci. 2015; 132: 41791.
105. Namur J, Chapot R, Pelage JP, Wassef M, Langevin F, Labarre D, et al. MR imaging detection of superparamagnetic iron oxide loaded tris-acryl embolization microspheres. J Vasc Interv Radiol. 2007; 18: 1287-95.
106. Lee KH, Liapi E, Vossen JA, Buijs M, Ventura VP, Georgiades C, et al. Distribution of iron oxide-containing embosphere particles after transcatheter arterial embolization in an animal model of liver cancer: Evaluation with MR imaging and implication for therapy. J Vasc Interv Radiol. 2008; 19: 1490-6.
107. Cilliers R, Song Y, Kohlmeir EK, Larson AC, Omary RA, Meade TJ. Modification of embolic-PVA particles with MR contrast agents. Magn Reson Med. 2008; 59: 898-902.
108. Chung EY, Kim HM, Lee GH, Kwak BK, Jung JS, Kuh HJ, et al. Design of deformable chitosan microspheres loaded with superparamagnetic iron oxide nanoparticles for embolotherapy detectable by magnetic resonance imaging. Carbohydr Polym. 2012; 90: 1725-31.
109. van Elk M, Lorenzato C, Ozbakir B, Oerlemans C, Storm G, Nijsen F, et al. Alginate microgels loaded with temperature sensitive liposomes for magnetic resonance imageable drug release and microgel visualization. Eur Polym J. 2015; 72: 620-31.
110. Zielhuis SW, Seppenwoolde JH, Bakker CJ, Jahnz U, Zonnenberg BA, van het Schip AD, et al. Characterization of holmium loaded alginate microspheres for multimodality imaging and therapeutic applications. J Biomed Mater Res A. 2007; 82: 892-8.
111. Oerlemans C, Seevinck PR, Smits ML, Hennink WE, Bakker CJ, van den Bosch MA, et al. Holmium-lipiodol-alginate microspheres for fluoroscopy-guided embolotherapy and multimodality imaging. Int J Pharm. 2015; 482: 47-53.
112. Wang Q, Qian K, Liu S, Yang Y, Liang B, Zheng C, et al. X-ray visible and uniform alginate microspheres loaded with *in situ* synthesized $BaSO_4$ nanoparticles for *in vivo* transcatheter arterial embolization. Biomacromolecules. 2015; 16: 1240-6.
113. Bartling SH, Budjan J, Aviv H, Haneder S, Kraenzlin B, Michaely H, et al. First multimodal embolization particles visible on x-ray/computed tomography and magnetic resonance imaging. Invest Radiol. 2011; 46: 178.
114. Stampfl U, Sommer CM, Bellemann N, Holzschuh M, Kueller A, Bluemmel J, et al. Multimodal visibility of a modified polyzene-f-coated spherical embolic agent for liver embolization: Feasibility study in a porcine model. J Vasc Interv Radiol. 2012; 23: 1225-31.
115. Sharma KV, Dreher MR, Tang Y, Pritchard W, Chiesa OA, Karanian J, et al. Development of "imageable" beads for transcatheter embolotherapy. J Vasc Interv Radiol. 2010; 21: 865-76.
116. Dreher MR, Sharma KV, Woods DL, Reddy G, Tang Y, Pritchard WF, et al. Radiopaque drug-eluting beads for transcatheter embolotherapy: Experimental study of drug penetration and coverage in swine. J Vasc Interv Radiol. 2012; 23: 257-64
117. Tacher V, Duran R, Lin M, Sohn JH, Sharma KV, Wang Z, et al. Multimodality imaging of ethiodized oil–loaded radiopaque microspheres during transarterial embolization of rabbits with VX2 liver tumors. Radiology. 2016; 279: 741-53.
118. Negussie AH, Dreher MR, Johnson CG, Tang Y, Lewis AL, Storm G, et al. Synthesis and characterization of image-able polyvinyl alcohol microspheres for image-guided chemoembolization. J Mater Sci Mater Med. 2015; 26: 198.
119. Duran R, Sharma K, Dreher MR, Ashrafi K, Mirpour S, Lin M, et al. A novel inherently radiopaque bead for transarterial embolization to treat liver cancer - a pre-clinical study. Theranostics. 2016; 6: 28-39.
120. You Y, Wang Z, Ran H, Zheng Y, Wang D, Xu J, et al. Nanoparticle-enhanced synergistic HIFU ablation and transarterial chemoembolization for efficient cancer therapy. Nanoscale. 2016; 8: 4324-39.
121. Shi H, Niu M, Tan L, Liu T, Shao H, Fu C, et al. A smart all-in-one theranostic platform for CT imaging guided tumor microwave thermotherapy based on IL@ZrO_2 nanoparticles. Chemical Science. 2015; 6: 5016-26.
122. Levy EB, Krishnasamy VP, Lewis AL, Willis S, Macfarlane C, Anderson V, et al. First human experience with directly image-able iodinated embolization microbeads. Cardiovasc Intervent Radiol. 2016; 39: 1177-86.
123. Wang Q, Xiao A, Liu Y, Zou Q, Zhou Q, Wang H, et al. One-step preparation of nano-in-micro poly(vinyl alcohol) embolic microspheres and used for dual-modal T_1/T_2-weighted magnetic resonance imaging. Nanomedicine. 2018; 14: 2551-61.
124. Zou Q, Hou F, Wang H, Liao Y, Wang Q, Yang Y. Microfluidic one-step preparation of alginate microspheres encapsulated with *in situ*-formed bismuth sulfide nanoparticles and their photothermal effect. Eur Polym J. 2019; 115: 282-9.
125. Hou F, Zhu Y, Zou Q, Zhang C, Wang H, Liao Y, et al. One-step preparation of multifunctional alginate microspheres loaded with *in situ*-formed gold nanostars as a photothermal agent. Materials Chemistry Frontiers. 2019; 3: 2018-24.
126. Wu XM, Wang JF, Ji JS, Chen MG, Song JG. Evaluation of efficacy of transcatheter arterial chemoembolization for hepatocellular carcinoma using magnetic resonance diffusion-weighted imaging. Onco Targets Ther. 2017; 10: 1637-43.
127. Kamel IR, Bluemke DA, Eng J, Liapi E, Messersmith W, Reyes DK, et al. The role of functional MR imaging in the assessment of tumor response after chemoembolization in patients with hepatocellular carcinoma. J Vasc Interv Radiol. 2006; 17: 505-12.
128. Campbell-Washburn AE, Tavallaei MA, Pop M, Grant EK, Chubb H, Rhode K, et al. Real-time MRI guidance of cardiac interventions. J Magn Reson Imaging. 2017; 46: 935-50.
129. Ratnayaka K, Faranesh AZ, Hansen MS, Stine AM, Halabi M, Barbash IM, et al. Real-time MRI-guided right heart catheterization in adults using passive catheters. Eur Heart J. 2013; 34: 380-9.
130. Horvath KA, Li M, Mazilu D, Guttman MA, McVeigh ER. Real-time magnetic resonance imaging guidance for cardiovascular procedures. Semin Thorac Cardiovasc Surg. 2007; 19: 330-5.
131. Miller JG, Li M, Mazilu D, Hunt T, Horvath KA. Real-time magnetic resonance imaging-guided transcatheter aortic valve replacement. J Thorac Cardiovasc Surg. 2016; 151: 1269-77.
132. Eitel C, Hindricks G, Grothoff M, Gutberlet M, Sommer P. Catheter ablation guided by real-time MRI. Curr Cardiol Rep. 2014; 16: 511.
133. Candela-Canto S, Alamar M, Alaez C, Muchart J, Forero C, de la Gala C, et al. Highly realistic simulation for robot-assisted hypothalamic hamartoma real-time MRI-guided laser interstitial thermal therapy (LITT). Childs Nerv Syst. 2020; 36: 1131-42.
134. Ries M, de Senneville BD, Roujol S, Berber Y, Quesson B, Moonen C. Real-time 3d target tracking in MRI guided focused ultrasound ablations in moving tissues. Magn Reson Med. 2010; 64: 1704-12.
135. Quesson B, Laurent C, Maclair G, de Senneville BD, Mougenot C, Ries M, et al. Real-time volumetric MRI thermometry of focused ultrasound ablation *in vivo*: A feasibility study in pig liver and kidney. NMR Biomed. 2011; 24: 145-53.
136. Moses ZB, Lee TC, Huang KT, Guenette JP, Chi JH. MRI-guided cryoablation for metastatic spine disease: Intermediate-term clinical outcomes in 14 consecutive patients. J Neurosurg Spine. 2020; 32: 676-81.
137. Mutic S, Dempsey JF. The viewray system: Magnetic resonance-guided and controlled radiotherapy. Semin Radiat Oncol. 2014; 24: 196-9.
138. Rosenberg SA, Wojcieszynski A, Hullett C, Geurts M, Lubner SJ, LoConte NK, et al. Real-time MRI-guided radiotherapy for pancreatic cancer. Radiother Oncol. 2016; 119: S96.
139. Shen Z, Wu A, Chen X. Iron oxide nanoparticle based contrast agents for magnetic resonance imaging. Mol Pharm. 2017; 14: 1352-64.
140. Yan G-P, Robinson L, Hogg P. Magnetic resonance imaging contrast agents: Overview and perspectives. Radiography. 2007; 13: e5-e19.
141. Mendichovszky IA, Marks SD, Simcock CM, Olsen OE. Gadolinium and nephrogenic systemic fibrosis: Time to tighten practice. Pediatr Radiol. 2008; 38: 489-96;.
142. Stephen ZR, Kievit FM, Zhang M. Magnetite nanoparticles for medical MR imaging. Mater Today. 2011; 14: 330-8.
143. Ersoy H, Rybicki FJ. Biochemical safety profiles of gadolinium-based extracellular contrast agents and nephrogenic systemic fibrosis. J Magn Reson Imaging. 2007; 26: 1190-7.
144. Perazella MA. Current status of gadolinium toxicity in patients with kidney disease. Clin J Am Soc Nephrol. 2009; 4: 461-9.
145. Qiu S, Ge NJ, Sun DK, Zhao S, Sun JF, Guo ZB, et al. Synthesis and characterization of magnetic polyvinyl alcohol (PVA) hydrogel microspheres for the embolization of blood vessel. IEEE Trans Biomed Eng. 2016; 63: 730-6.
146. Wang H, Qin X-Y, Li Z-Y, Guo L-Y, Zheng Z-Z, Liu L-S, et al. Preparation and evaluation of MRI detectable poly (acrylic acid) microspheres loaded with superparamagnetic iron oxide nanoparticles for transcatheter arterial embolization. Int J Pharm. 2016; 511: 831-9.
147. Li Z-Y, Qin X-Y, Guo L-Y, Wang H, Liu X-X, Zheng Z-Z, et al. Poly(acrylic acid) microspheres loaded with superparamagnetic iron oxide nanoparticles for transcatheter arterial embolization and MRI detectability: *In vitro* and *in vivo* evaluation. Int J Pharm. 2017; 527: 31-41.
148. Li J, Wang J, Li J, Yang X, Wan J, Zheng C, et al. Fabrication of Fe_3O_4@PVA microspheres by one-step electrospray for magnetic resonance imaging during transcatheter arterial embolization. Acta Biomater. 2021; 131: 532-43.
149. Fernandez-Gutierrez F, Wolska-Krawczyk M, Buecker A, Houston JG, Melzer A. Workflow optimisation for multimodal imaging procedures: A case of combined X-ray and MRI-guided TACE. Minim Invasive Ther Allied Technol. 2017; 26: 31-8.
150. Kim DH, Li W, Chen J, Zhang Z, Green RM, Huang S, et al. Multimodal imaging of nanocomposite microspheres for transcatheter intra-arterial drug delivery to liver tumors. Sci Rep. 2016; 6: 29653.
151. Key J, Leary JF. Nanoparticles for multimodal *in vivo* imaging in nanomedicine. Int J Nanomedicine. 2014; 9: 711-26.
152. Mahnken AH. Current status of transarterial radioembolization. World J Radiol. 2016; 8: 449-59.

153. Dawson LA, Normolle D, Balter JM, McGinn CJ, Lawrence TS, Ten Haken RK. Analysis of radiation-induced liver disease using the lyman ntcp model. Int J Radiat Oncol Biol Phys. 2002; 53: 1422.
154. Dawson LA, McGinn CJ, Normolle D, Ten Haken RK, Walker S, Ensminger W, et al. Escalated focal liver radiation and concurrent hepatic artery fluorodeoxyuridine for unresectable intrahepatic malignancies. J Clin Oncol. 2000; 18: 2210-8.
155. Gulec SA, Fong Y. Yttrium 90 microsphere selective internal radiation treatment of hepatic colorectal metastases. Arch Surg. 2007; 142: 675-82.
156. Sacco R, Mismas V, Marceglia S, Romano A, Giacomelli L, Bertini M, et al. Transarterial radioembolization for hepatocellular carcinoma: An update and perspectives. World J Gastroenterol. 2015; 21: 6518-25.
157. Drescher R, Seifert P, Guhne F, Aschenbach R, Kuhnel C, Freesmeyer M. Radioembolization with holmium-166 polylactic acid microspheres: Distribution of residual activity in the delivery set and outflow dynamics during planning and treatment procedures. J Endovasc Ther. 2021; 28: 452-62.
158. De La Vega JC, Esquinas PL, Rodriguez-Rodriguez C, Bokharaei M, Moskalev I, Liu D, et al. Radioembolization of hepatocellular carcinoma with built-in dosimetry: First *in vivo* results with uniformly-sized, biodegradable microspheres labeled with ^{188}Re. Theranostics. 2019; 9: 868-83.
159. Biederman DM, Titano JJ, Tabori NE, Pierobon ES, Alshebeeb K, Schwartz M, et al. Outcomes of radioembolization in the treatment of hepatocellular carcinoma with portal vein invasion: Resin versus glass microspheres. J Vasc Interv Radiol. 2016; 27: 812-21
160. Mazzaferro V, Sposito C, Bhoori S, Romito R, Chiesa C, Morosi C, et al. Yttrium-90 radioembolization for intermediate-advanced hepatocellular carcinoma: A phase 2 study. Hepatology. 2013; 57: 1826-37.
161. Moreno-Luna LE, Yang JD, Sanchez W, Paz-Fumagalli R, Harnois DM, Mettler TA, et al. Efficacy and safety of transarterial radioembolization versus chemoembolization in patients with hepatocellular carcinoma. Cardiovasc Intervent Radiol. 2013; 36: 714-23.
162. Rognoni C, Ciani O, Sommariva S, Facciorusso A, Tarricone R, Bhoori S, et al. Trans-arterial radioembolization in intermediate-advanced hepatocellular carcinoma: Systematic review and meta-analyses. Oncotarget. 2016; 7: 72343-55.
163. Saini A, Wallace A, Alzubaidi S, Knuttinen MG, Naidu S, Sheth R, et al. History and evolution of yttrium-90 radioembolization for hepatocellular carcinoma. J Clin Med. 2019; 8: 55.
164. Nabrinsky E, James E. Highlighting survival with yttrium-90 radioembolization therapy in unresectable hepatocellular carcinoma. Cureus. 2020; 12: e8163.
165. Abdel-Rahman O, Elsayed Z. Yttrium-90 microsphere radioembolisation for unresectable hepatocellular carcinoma. Cochrane Database Syst Rev. 2020; 1: CD011313.
166. Salem R, Gordon AC, Mouli S, Hickey R, Kallini J, Gabr A, et al. Y90 radioembolization significantly prolongs time to progression compared with chemoembolization in patients with hepatocellular carcinoma. Gastroenterology. 2016; 151: 1155-63.
167. Toskich B, Patel T. Radioembolization for hepatocellular carcinoma: The time has come. Hepatology. 2018; 67: 820-2.
168. Sangro B, Inarrairaegui M, Bilbao JI. Radioembolization for hepatocellular carcinoma. J Hepatol. 2012; 56: 464-73.
169. Boas FE, Bodei L, Sofocleous CT. Radioembolization of colorectal liver metastases: Indications, technique, and outcomes. J Nucl Med. 2017; 58: 104S-11S.
170. Wang S, Yang C, Zhang J, Kong XR, Zhu H, Wu F, et al. First experience of high-intensity focused ultrasound combined with transcatheter arterial embolization as local control for hepatoblastoma. Hepatology. 2014; 59: 170-7.
171. Liang YJ, Yu H, Feng G, Zhuang L, Xi W, Ma M, et al. High-performance poly(lactic-co-glycolic acid)-magnetic microspheres prepared by rotating membrane emulsification for transcatheter arterial embolization and magnetic ablation in VX2 liver tumors. ACS Appl Mater Interfaces. 2017; 9: 43478-89.
172. Galanakis N, Kehagias E, Matthaiou N, Samonakis D, Tsetis D. Transcatheter arterial chemoembolization combined with radiofrequency or microwave ablation for hepatocellular carcinoma: A review. Hepatic Oncology. 2018; 5: HEP07.
173. Ni JY, Sun HL, Luo JH, Jiang XY, Chen D, Wang WD, et al. Transarterial chemoembolization and sorafenib combined with microwave ablation for advanced primary hepatocellular carcinoma: A preliminary investigation of safety and efficacy. Cancer Manag Res. 2019; 11: 9939-50.
174. Sun M, Shang P, Bai J, Li S, Li M. High-intensity focused ultrasound ablation combined with transcatheter arterial chemoembolization improves long-term efficacy and prognosis of primary liver cancer. J Clin Lab Anal. 2021; 35: e23633.
175. Zangos S, Eichler K, Balzer JO, Straub R, Hammerstingl R, Herzog C, et al. Large-sized hepatocellular carcinoma (HCC): A neoadjuvant treatment protocol with repetitive transarterial chemoembolization (TACE) before percutaneous MR-guided laser-induced thermotherapy (litt). Eur Radiol. 2007; 17: 553-63.
176. Sheth RA, Wen X, Li J, Melancon MP, Ji X, Andrew Wang Y, et al. Doxorubicin-loaded hollow gold nanospheres for dual photothermal ablation and chemoembolization therapy. Cancer Nanotechnol. 2020; 11: 6.
177. Xie H, Wang H, An W, Ma W, Qi R, Yang B, et al. The efficacy of radiofrequency ablation combined with transcatheter arterial chemoembolization for primary hepatocellular carcinoma in a cohort of 487 patients. PLoS One. 2014; 9: e89081.
178. Nishikawa H, Kimura T, Kita R, Osaki Y. Radiofrequency ablation for hepatocellular carcinoma. Int J Hyperthermia. 2013; 29: 558-68.
179. Lewis AR, Padula CA, McKinney JM, Toskich BB. Ablation plus transarterial embolic therapy for hepatocellular carcinoma larger than 3 cm: Science, evidence, and future directions. Semin Intervent Radiol. 2019; 36: 303-9.
180. Li W, Ni C-F. Current status of the combination therapy of transarterial chemoembolization and local ablation for hepatocellular carcinoma. Abdominal Radiology. 2019; 44: 2268-75.
181. Liao M, Huang J, Zhang T, Wu H. Transarterial chemoembolization in combination with local therapies for hepatocellular carcinoma: A meta-analysis. PLoS One. 2013; 8: e68453.
182. Moroz P, Jones SK, Gray BN. Tumor response to arterial embolization hyperthermia and direct injection hyperthermia in a rabbit liver tumor model. J Surg Oncol. 2002; 80: 149-56.
183. Li L, Guo X, Peng X, Zhang H, Liu Y, Li H, et al. Radiofrequency-responsive dual-valent gold nanoclusters for enhancing synergistic therapy of tumor ablation and artery embolization. Nano Today. 2020; 35: 100934.
184. Moroz P, Jones SK, Gray BN. Status of hyperthermia in the treatment of advanced liver cancer. J Surg Oncol. 2001; 77: 259-69.
185. Rajan A, Sahu NK. Review on magnetic nanoparticle-mediated hyperthermia for cancer therapy. J Nanopart Res. 2020; 22: 319.
186. Liang Y-J, Wang H, Yu H, Feng G, Liu F, Ma M, et al. Magnetic navigation helps PLGA drug loaded magnetic microspheres achieve precise chemoembolization and hyperthermia. Colloids Surf Physicochem Eng Aspects. 2020; 588: 124364.
187. Takamatsu S, Matsui O, Gabata T, Kobayashi S, Okuda M, Ougi T, et al. Selective induction hyperthermia following transcatheter arterial embolization with a mixture of nano-sized magnetic particles (ferucarbotran) and embolic materials: Feasibility study in rabbits. Radiat Med. 2008; 26: 179-87.
188. Yu H, Zhu GY, Xu RZ, Niu HZ, Lu Q, Li GZ, et al. Arterial embolization hyperthermia using as2o3 nanoparticles in VX2 carcinoma-induced liver tumors. PLoS One. 2011; 6: e17926.
189. Wu J, Wang H, Zhang H, Wei L, Wang X, Wang X, et al. Stainless steel hollow microspheres for arterial embolization hyperthermia. Journal of Medical and Biological Engineering. 2017; 37: 810-9.
190. Smolkova IS, Kazantseva NE, Makoveckaya KN, Smolka P, Saha P, Granov AM. Maghemite based silicone composite for arterial embolization hyperthermia. Mater Sci Eng, C. 2015; 48: 632-41.
191. Li Z, Kawashita M, Araki N, Mitsumori M, Hiraoka M, Doi M. Magnetic sio2 gel microspheres for arterial embolization hyperthermia. Biomed Mater. 2010; 5: 065010.
192. Zhou YF. High intensity focused ultrasound in clinical tumor ablation. World J Clin Oncol. 2011; 2: 8-27.
193. Jin C, Zhu H, Wang Z, Wu F, Chen W, Li K, et al. High-intensity focused ultrasound combined with transarterial chemoembolization for unresectable hepatocellular carcinoma: Long-term follow-up and clinical analysis. Eur J Radiol. 2011; 80: 662-9.
194. Chen B, Chen J, Luo Q, Guo C. Effective strategy of the combination of high-intensity focused ultrasound and transarterial chemoembolization for improving outcome of unresectable and metastatic hepatoblastoma: A retrospective cohort study. Transl Oncol. 2014; 7: 788-94.
195. Luo Y, Jiang Y. Comparison of efficiency of TACE plus HIFU and TACE alone on patients with primary liver cancer. JCPSP. 2019; 29: 414-7.
196. Hu H, Chen GF, Yuan W, Wang JH, Zhai B. Microwave ablation with chemoembolization for large hepatocellular carcinoma in patients with cirrhosis. Int J Hyperthermia. 2018; 34: 1351-8.
197. Chen QF, Jia ZY, Yang ZQ, Fan WL, Shi HB. Transarterial chemoembolization monotherapy versus combined transarterial chemoembolization-microwave ablation therapy for hepatocellular carcinoma tumors ≤ 5 cm: A propensity analysis at a single center. Cardiovasc Intervent Radiol. 2017; 40: 1748-55.
198. Sheta E, El-Kalla F, El-Gharib M, Kobtan A, Elhendawy M, Abd-Elsalam S, et al. Comparison of single-session transarterial chemoembolization combined with microwave ablation or radiofrequency ablation in the treatment of hepatocellular carcinoma: A randomized-controlled study. Eur J Gastroenterol Hepatol. 2016; 28: 1198-203.
199. Ginsburg M, Zivin SP, Wroblewski K, Doshi T, Vasnani RJ, Van Ha TG. Comparison of combination therapies in the management of hepatocellular carcinoma: Transarterial chemoembolization with radiofrequency ablation versus microwave ablation. J Vasc Interv Radiol. 2015; 26: 330-41.
200. Mao J, Tang S, Hong D, Zhao F, Niu M, Han X, et al. Therapeutic efficacy of novel microwave-sensitized mpeg-PLGA@ZrO_2@(DOX + ILS) drug-loaded microspheres in rabbit VX2 liver tumours. Nanoscale. 2017; 9: 3429-39.
201. Du Q, Fu C, Tie J, Liu T, Li L, Ren X, et al. Gelatin microcapsules for enhanced microwave tumor hyperthermia. Nanoscale. 2015; 7: 3147-54.
202. Shi H, Liu T, Fu C, Li L, Tan L, Wang J, et al. Insights into a microwave susceptible agent for minimally invasive microwave tumor thermal therapy. Biomaterials. 2015; 44: 91-102.
203. Wu Q, Xia N, Long D, Tan L, Rao W, Yu J, et al. Dual-functional supernanoparticles with microwave dynamic therapy and microwave thermal therapy. Nano Lett. 2019; 19: 5277-86.
204. Pacella CM, Bizzarri G, Cecconi P, Caspani B, Magnolfi F, Bianchini A, et al. Hepatocellular carcinoma: Long-term results of combined treatment with laser

thermal ablation and transcatheter arterial chemoembolization. Radiology. 2001; 219: 669-78.
205. Ferrari FS, Stella A, Gambacorta D, Magnolfi F, Fantozzi F, Pasquinucci P, et al. Treatment of large hepatocellular carcinoma: Comparison between techniques and long term results. Radiol Med. 2004; 108: 356-71.
206. Huang D, Dai H, Tang K, Chen B, Zhu H, Chen D, et al. A versatile ucst-type composite microsphere for image-guided chemoembolization and photothermal therapy against liver cancer. Nanoscale. 2020; 12: 20002-15.
207. Zhou J, Ling G, Cao J, Ding X, Liao X, Wu M, et al. Transcatheter intra-arterial infusion combined with interventional photothermal therapy for the treatment of hepatocellular carcinoma. Int J Nanomedicine. 2020; 15: 1373-85.
208. Chen L, Sun J, Yang X. Radiofrequency ablation-combined multimodel therapies for hepatocellular carcinoma: Current status. Cancer Lett. 2016; 370: 78-84.
209. Yang D, Luo K, Liu H, Cai B, Tao G, Su X, et al. Meta-analysis of transcatheter arterial chemoembolization plus radiofrequency ablation versus transcatheter arterial chemoembolization alone for hepatocellular carcinoma. Oncotarget. 2016; 8: 2960-70.
210. Chen Q, Ying H, Gao S, Shen Y, Meng Z, Chen H, et al. Radiofrequency ablation plus chemoembolization versus radiofrequency ablation alone for hepatocellular carcinoma: A systematic review and meta-analysis. Clin Res Hepatol Gastroenterol. 2016; 40: 309-14.
211. Li L, Zhang H, Zhao H, Shi D, Zheng C, Zhao Y, et al. Radiofrequency-thermal effect of cisplatin-crosslinked nanogels for triple therapies of ablation-chemo-embolization. Chem Eng J. 2022; 450: 138421.
212. Tsoi KM, MacParland SA, Ma XZ, Spetzler VN, Echeverri J, Ouyang B, et al. Mechanism of hard-nanomaterial clearance by the liver. Nat Mater. 2016; 15: 1212-21.
213. Chithrani BD, Chan WCW. Elucidating the mechanism of cellular uptake and removal of protein-coated gold nanoparticles of different sizes and shapes. Nano Lett. 2007; 7: 1542-50.
214. Fernando I, Zhou Y. Impact of ph on the stability, dissolution and aggregation kinetics of silver nanoparticles. Chemosphere. 2019; 216: 297-305.
215. Wang Z, Liu G, Zheng H, Chen X. Rigid nanoparticle-based delivery of anti-cancer sirna: Challenges and opportunities. Biotechnol Adv. 2014; 32: 831-43.
216. Sun X, Sun M, Liu M, Yuan B, Gao W, Rao W, et al. Shape tunable gallium nanorods mediated tumor enhanced ablation through near-infrared photothermal therapy. Nanoscale. 2019; 11: 2655-67.
217. Yan J, Lu Y, Chen G, Yang M, Gu Z. Advances in liquid metals for biomedical applications. Chem Soc Rev. 2018; 47: 2518-33.
218. Zhang M, Yao S, Rao W, Liu J. Transformable soft liquid metal micro/nanomaterials. Materials Science and Engineering: R: Reports. 2019; 138: 1-35.
219. Chechetka SA, Yu Y, Zhen X, Pramanik M, Pu K, Miyako E. Light-driven liquid metal nanotransformers for biomedical theranostics. Nat Commun. 2017; 8: 15432.
220. Wang Q, Yu Y, Pan K, Liu J. Liquid metal angiography for mega contrast X-ray visualization of vascular network in reconstructing in-vitro organ anatomy. IEEE Trans Biomed Eng. 2014; 61: 2161.
221. Wang Q, Yu Y, Liu J. Delivery of liquid metal to the target vessels as vascular embolic agent to starve diseased tissues or tumors to death. arXiv preprint. 2014.
222. Fan L, Duan M, Xie Z, Pan K, Wang X, Sun X, et al. Injectable and radiopaque liquid metal/calcium alginate hydrogels for endovascular embolization and tumor embolotherapy. Small. 2019; 16: 1903421.
223. Duan M, Zhu X, Fan L, He Y, Yang C, Guo R, et al. Phase-transitional bismuth-based metals enable rapid embolotherapy, hyperthermia, and biomedical imaging. Adv Mater. 2022; 34: 2205002.
224. Wang D, Wu Q, Guo R, Lu C, Niu M, Rao W. Magnetic liquid metal loaded nano-in-micro spheres as fully flexible theranostic agents for smart embolization. Nanoscale. 2021; 13: 8817-36.
225. Wang D, Rao W. Alginate sponge assisted instantize liquid metal nanocomposite for photothermo-chemotherapy. Applied Materials Today. 2022; 29: 101583.
226. Oloye O, Riches JD, O'Mullane AP. Liquid metal assisted sonocatalytic degradation of organic azo dyes to solid carbon particles. Chem Commun. 2021; 57: 9296-9.
227. Sun X, Yuan B, Rao W, Liu J. Amorphous liquid metal electrodes enabled conformable electrochemical therapy of tumors. Biomaterials. 2017; 146: 156-67.
228. Li S, Jiang Q, Liu S, Zhang Y, Tian Y, Song C, et al. A DNA nanorobot functions as a cancer therapeutic in response to a molecular trigger *in vivo*. Nat Biotechnol. 2018; 36: 258-64.
229. Ayaru L, Pereira SP, Alisa A, Pathan AA, Williams R, Davidson B, et al. Unmasking of alpha-fetoprotein-specific CD^{4+} T cell responses in hepatocellular carcinoma patients undergoing embolization. J Immunol. 2007; 178: 1914-22.